AFRL-VA-WP-TR-1999-3047

SMART ACTUATION SYSTEMS FOR ENHANCED AIRCRAFT MANEUVER PERFORMANCE

K. APPA
J. AUSMAN

Northrop Grumman Corporation
Military Aircraft Systems Division
One Hornet Way
El Segundo, CA 90245-2804

N. S. KHOT

Air Vehicles Directorate (VASD/AFRL)
Air Force Research Laboratory
Air Force Materiel Command
Wright-Patterson Air Force Base, Ohio 45433-7542

OCTOBER 1998

Final Report for Period July 1997 to October 1998

AIR VEHICLES DIRECTORATE
AIR FORCE RESEARCH LABORATORY
AIR FORCE MATERIEL COMMAND
WRIGHT- PATTERSON AIR FORCE BASE, OHIO 45433-7542

NOTICE

WHEN GOVERNMENT DRAWINGS, SPECIFICATIONS, OR OTHER DATA ARE USED FOR ANY PURPOSE OTHER THAN IN CONNECTION WITH DEFINITE GOVERNMENT-RELATED PROCUREMENT, THE UNITED STATES GOVERNMENT INCURS NO RESPONSIBILITY OR ANY OBLIGATION WHATSOEVER. THE FACT THAT THE GOVERNMENT MAY HAVE FORMULATED OR IN ANY WAY SUPPLIED THE SAID DRAWING, SPECIFICATIONS, OR OTHER DATA, IS NOT TO BE REGARDED BY IMPLICATIONS, OR OTHERWISE IN ANY MANNER CONSTRUED, AS LICENSING THE HOLDER, OR ANY OTHER PERSON OR CORPORATION; OR AS CONVEYING ANY RIGHTS OR PERMISSION TO MANUFACTURE, USE, OR SELL ANY PATENTED INVENTION THAT MAY IN ANY WAY BE RELATED THERETO.

THIS REPORT IS RELEASEABLE TO THE NATIONAL TECHNICAL INFORMATION SERVICE (NITS), AT NTIS IT WILL BE AVAILABLE TO THE GENERAL PUBLIC, INCLUDING FOREIGN NATION.

THIS TECHNICAL REPORT HAS BEEN REVIEWED AND IS APPROVED FOR PUBLICATION.

Narendra S. Khot 2 April 99

Narendra S. Khot
Project Engineer
Design and Analysis Branch
Structures Division

Nelson D. Wolf

Nelson D. Wolf, Chief
Design and Analysis Branch
Structures Division

J. L. M. Manter

JOSEPH M. MANTER
Chief
Structures Division

IF YOUR ADDRESS HAS CHANGED, IF YOU WISH TO BE REMOVED FROM OUR MAILING LIST, OR IF THE ADDRESSEE IS NO LONGER EMPLOYED BY YOUR ORGANIZATION, PLEASE NOTIFY AFRL/VASD BLDG 146, 2210 8TH STREET, WPAFB OH 45433-7531

REPORT DOCUMENTATION PAGE	Form Approved OMB No. 0704-0188

1. AGENCY USE ONLY *(Leave blank)*	2. REPORT DATE	3. REPORT TYPE AND DATES COVERED
	01 October 1998	Final, 6-15-97 to 10-30-98

4. TITLE AND SUBTITLE

Smart Actuation Systems for Enhanced Aircraft Maneuver Performance

5. FUNDING NUMBERS

C: F33615-95-2-3215
PE: 62201
PR: 2401
TA: ST
WU: AP

6. AUTHOR(S)

K. Appa, J. Ausman, and N.S. Khot

7. PERFORMING ORGANIZATION NAME(S) AND ADDRESS(ES)

Northrop Grumman Corporation
One Hornet Way
El Segundo, California 90245-2804

8. PERFORMING ORGANIZATION REPORT NUMBER

9. SPONSORING / MONITORING AGENCY NAME(S) AND ADDRESS(ES)

AIR VEHICLES DIRECTORATE
AIR FORCE RESEARCH LABORATORY
AIR FORCE MATERIEL COMMAND
WRIGHT- PATTERSON AIR FORCE BASE, OHIO 45433-7542
POC: N.S. Khot, 937-255-6992

10. SPONSORING / MONITORING AGENCY REPORT NUMBER

AFRL-VA-WP-TR-1999-3047

11. SUPPLEMENTARY NOTES

12a. DISTRIBUTION / AVAILABILITY STATEMENT

Approved for Public Release; Distribution Unlimited

12b.

13. ABSTRACT (Maximum 200 Words)

The final report describes an analytical development of a simulation algorithm based on the optimal control theory to compute flight maneuver loads using solid state actuators. A state space formulation including steady and unsteady air loads, and closed loop control laws has been derived to perform aeroelastic analyses and flight dynamics of flexible aircraft. The algorithm uses the Air Force sponsored optimization software, ASTROS, to generate necessary structural and aerodynamic data. A few flight maneuver cases have been exercised to show how a small amount of actuator power can perform 6.0 g pull-up maneuver of an aircraft of the size of F16 when distributed solid state actuators are used. This study also suggests that the solid state actuators must be able to travel large distances between contact points for minimum actuator power. Such large displacements and forces are achievable in piezoelectric devices such as the inchworm actuators.

14. SUBJECT TERMS

Smart Actuation System, Feasibility Study, Optimal Control, Aircraft Maneuver

15. NUMBER OF PAGES 64

16. PRICE CODE

17. SECURITY CLASSIFICATION OF REPORT	18. SECURITY CLASSIFICATION OF THIS PAGE	19. SECURITY CLASSIFICATION OF ABSTRACT	20. LIMITATION OF ABSTRACT
Unclassified	Unclassified	Unclassified	SAR

TABLE OF CONTENTS

PREFACE

This report describes work performed by the Advanced Structural Methods department of the Northrop Grumman Corporation, Military Aircraft Systems Division, for the Air Vehicles Directorate of Air Force Research Laboratory, Air Force Materiel Command, Wright-Patterson Air Force Base, Ohio, under contract F33615-95-D-3215, Project No. 0006, "Smart Actuation Systems for Enhanced Aircraft Maneuver Performance."

The optimal control theory is applied to determine the solid state actuator placement and to calculate the forces required to perform flight maneuvers of flexible aircraft at desired conditions. The algorithm uses the Air Force sponsored optimization software, ASTROS, to generate structural and aerodynamic data. A few flight maneuver cases have been exercised to show the merits of solid state actuators in 6.0g pull-up of a typical fighter aircraft.

Dr. Narendra S. Khot, at Air Vehicles Directorate, Air Force Research Laboratory, initiated the solid state actuator feasibility study program and served as the technical monitor. Dr. Kari Appa was the principal investigator. Mr. John Ausman was responsible for implementing the optimal control algorithm in conjunction with the ASTROS module to generate required data.

1. INTRODUCTION

1.1 Summary

The performance characteristics of aircraft largely depend on the quality and distribution of airflow on the lifting surfaces. By nature, birds are able to configure their wings in such a manner that the airflow quality and flying efficiency are at optimum conditions. Duplication of such airflow characteristics on manufactured flying vehicles has been a desired objective of airplane designers, beginning with the Wright brothers. To simulate bird-like flying characteristics, the lifting surfaces must be able to deform smoothly at appropriate locations. In the mid 1980s, the Air Force sponsored a mission adaptive wing (MAW) project to study aerodynamic and maneuver performance characteristics of tactical aircraft (Refs. 1, 2 and 3). An F-111 aircraft was selected and fitted with hydraulic actuators to deform the wing. This aircraft was test flown in several mission performances. The test results showed overwhelming aerodynamic performance benefits and agility characteristics. However, the actuation system was heavy and expensive to operate so practical implementation of this concept could not be realized at that time.

Recent analytical and wind tunnel studies sponsored by ARPA and the Air Force (Ref. 4) show how smoothly contoured control surfaces promote incremental growth in suction pressure near the leading edge. This has a beneficial effect on control surface effectiveness, leading to enhanced aircraft maneuver performance. A few test cases taken from this study are presented in the next section to emphasize the need for active control of lifting surface camber to enhance aircraft performance. This report, in subsequent sections, describes an analytical approach, which can be used to determine optimum wing camber, and also to command the solid state actuators to deform the desired lifting surface at reduced power requirement.

1.2 Technical Background

In conventional aircraft, the leading and trailing edge control surfaces are used, as aerodynamic effectors to generate desired lift distributions on wings and control surfaces. The leading edges are generally used to minimize flow separation at moderately high angle of attack flight maneuver cases, while the trailing edges are used to obtain desired pitching and rolling moments.

Two factors limit the effectiveness of the trailing edge control surfaces. First, the control effectiveness decreases with increasing dynamic pressure due to aeroelastic effects (i.e. adverse twisting of the wing). The second problem is that there exists a massive flow separation along the hinge line, resulting in reduced aerodynamic loading on the wing as well as on the control surface. Figure 1-1a shows flow separation due to rapid

change in control surface slope at the hinge line. This problem can be alleviated by the use of hingeless contoured trailing edge surface as shown in Figure 1-1b.

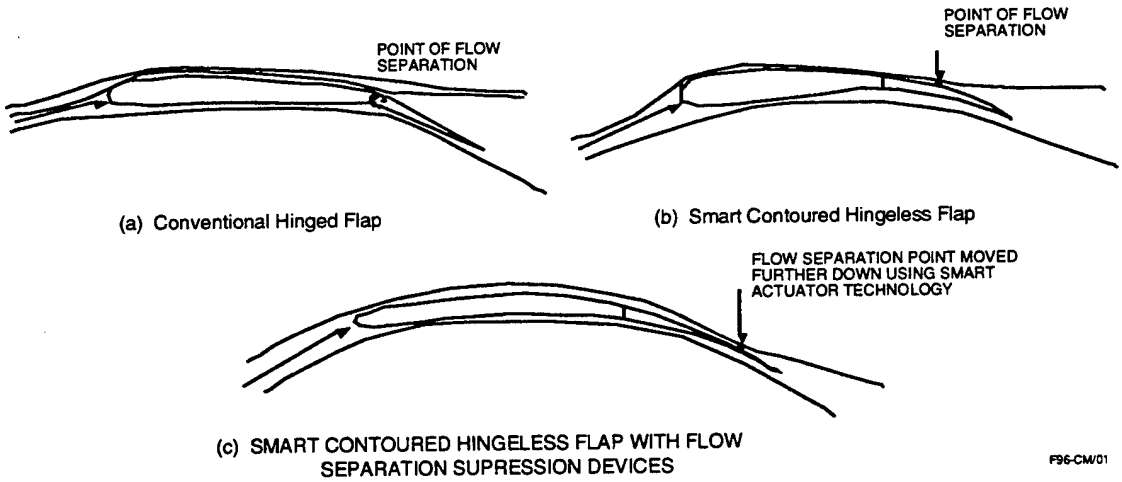

Figure 1-1. Flow Characteristics over Hinged and Hingeless Contoured Control Surfaces

Further, a flow separation suppression device can be used to move the point of separation towards the trailing edge as depicted in Figure 1-1c. To demonstrate the difference in pressure distributions between hinged flap and smoothly contoured flaps, a few studies were conducted using computational fluid dynamics (CFD) method. The computational (CFD) solutions are shown in Figure 1-2 in which the solid curve represents the pressure distribution computed for contoured trailing edge surface, while the dotted curve denotes the data obtained using a hinged flap

Subsequently, wind tunnel tests were conducted in NASA Langley's Transonic Dynamic Tunnel (TDT) under a contract (F33615-93-C-3202), "Smart Materials and Structures - Smart Wing" sponsored by DARPA.

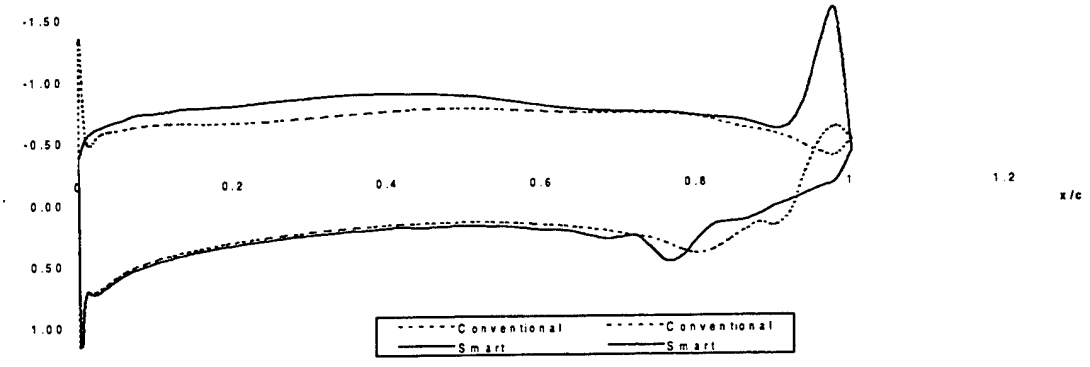

Figure 1-2. Comparison of Pressure Distribution between Hinged and Hingeless Contoured Control Surfaces

The hinged flap data depict flow separation at the trailing edge, whereas the contoured flap shows large suction pressure on the flap, as well as on most of the upper surface. This type of pressure distribution has some beneficial effects on aeroelastic stability. Since the elastic axis lies downstream of the section aerodynamic center, the increased load near the leading edge twists the wing upwards, resulting in an increased angle of attack relative to that observed in the case of a conventional trailing edge flap. Thus, the effectiveness of the trailing edge control surface increases with increased dynamic pressure, and consequently, the roll reversal speed increases. This is a significant contrast to the case of traditional control surfaces where the agility of the aircraft is reduced with increasing dynamic pressure.

In the case of wind tunnel tests, two models were constructed. One model had conventional hinged trailing edge flaps and ailerons, while the other (also known as the Smart Wing) had deformable control surfaces made of shape memory alloys (SMA). Typical wind tunnel results are presented in Figures 1-3 through 1-5. The trends are similar to those observed in the CFD solutions. However, due to lack of instrumentation, the pressure loop for the hinged control surface was not observed in the wind tunnel data.

Aerodynamic coefficients (both lift and rolling moment) due to aileron deflection were measured in the wind tunnel. The measured data was used to compute the roll reversal speed shown in Figure 1-6. The roll reversal speed is the velocity at which the aileron effectiveness is equal to zero. As expected, the hingeless control surface yields higher roll rate and higher control reversal speed compared to the hinged control surface.

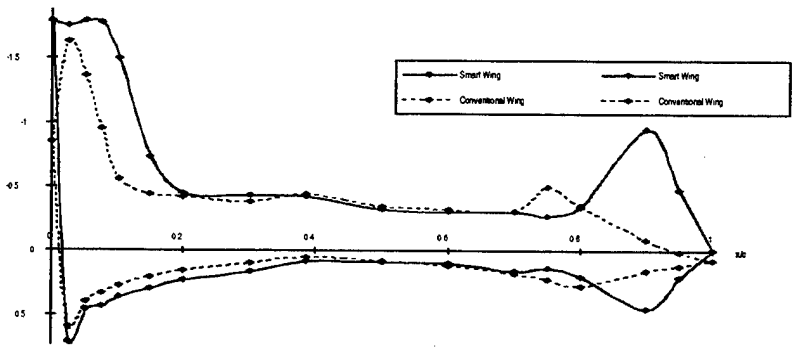

Figure 1-3. Pressure Coefficient (CP) Comparison, at 36% Span
Q = 60 psf, a = 8°, Flap = 10°, Aileron = 0°(Run 100 vs. 80)

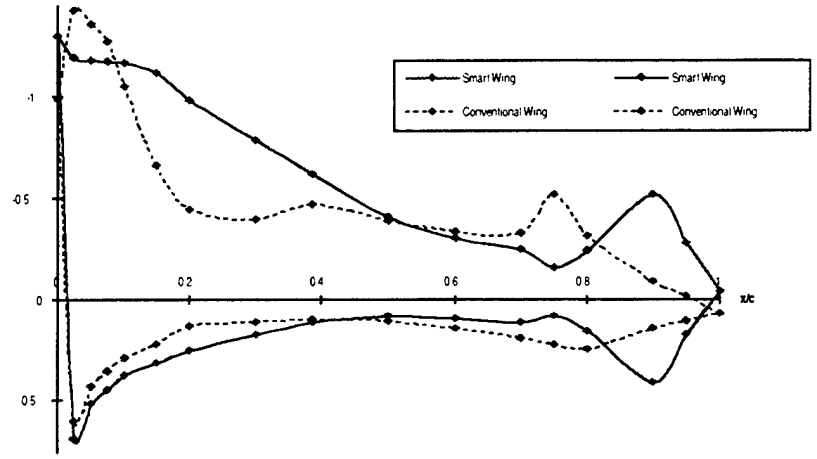

Figure 1-4. Pressure Coefficient (CP) Comparison, at 50% Span
Q = 60 psf, a = 8°, Flap = 10°, Aileron = 0°(Run 100 vs. 80)

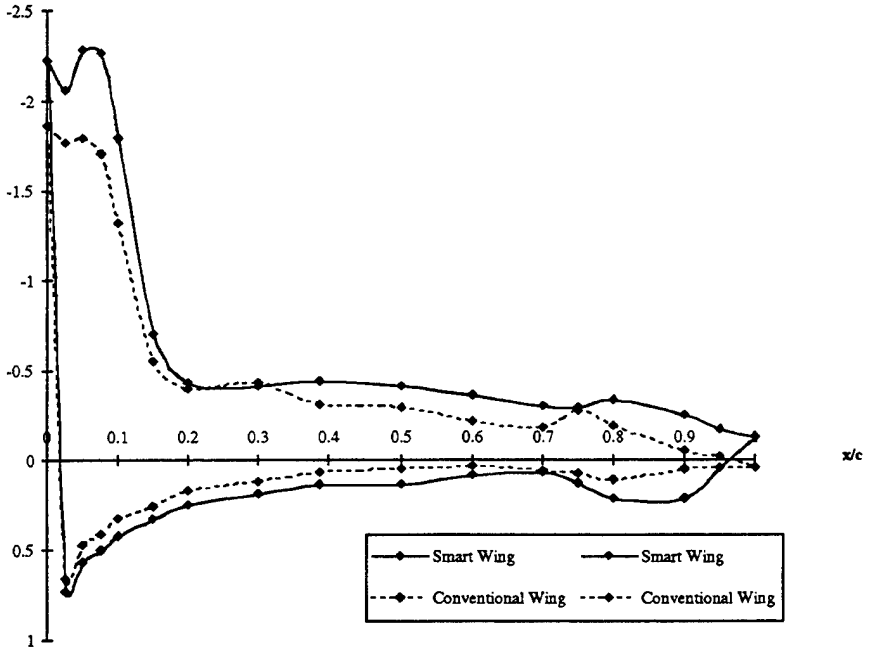

Figure 1-5. Pressure Coefficient (CP) Comparison, at 80% Span
Q = 120 psf, a = 8°, Flap = 0°, Aileron = 0°(Run 109 vs. 20)

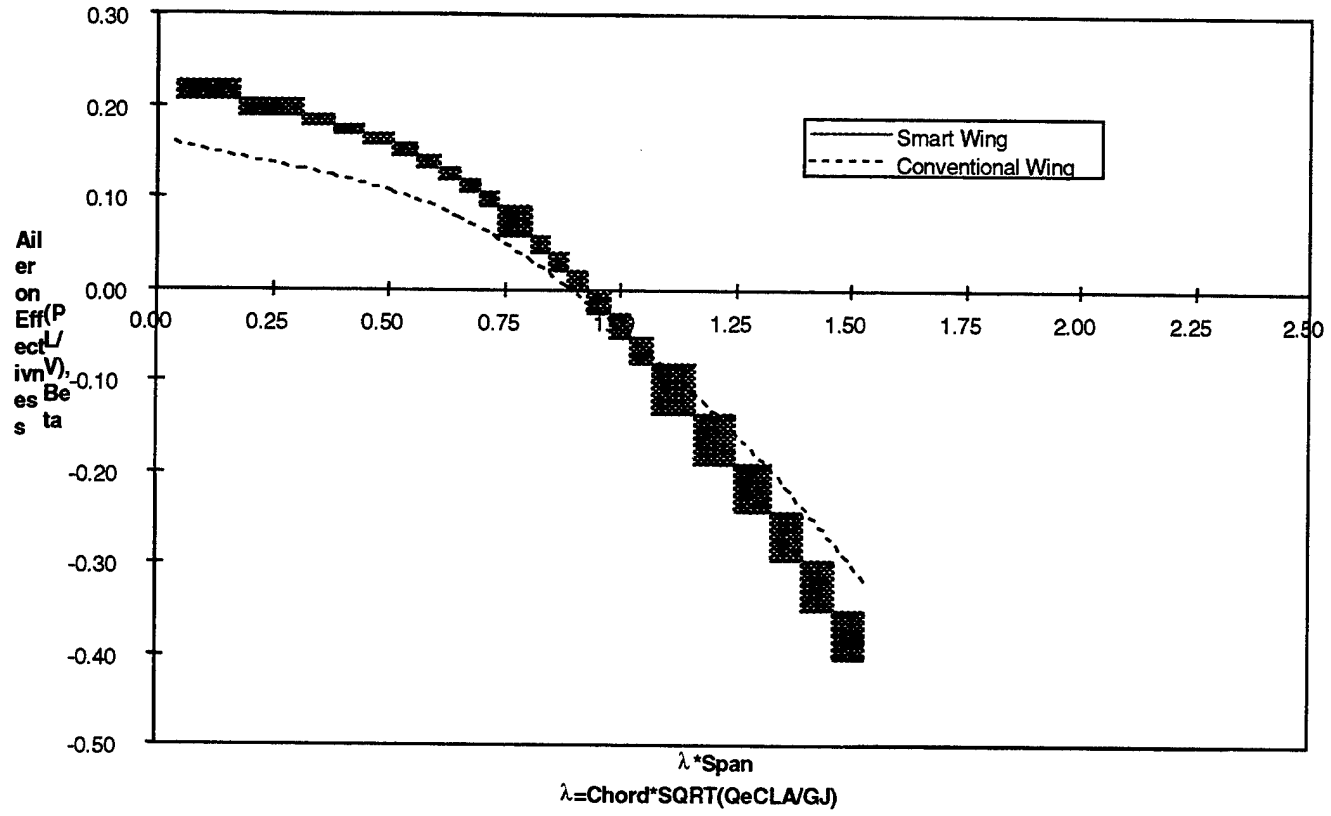

Figure 1-6. Aileron effectiveness Vs. Nondimensional Dynamic Pressure

Thus, hingeless control surfaces offer many improvements over the traditional control surfaces. Chief among these improvements is the improved aerodynamic performance. Hence, there is a compelling reason to investigate various avenues, in the light of smart structures technology, to develop feasible mechanisms to control the camber of lifting surfaces as is desired in any combat mission.

Today, with the advent of new materials technology, it is possible to design smoothly deforming lifting surfaces using composite materials. Solid state actuators, which can output large forces at rates used in modern flight control algorithms, are also being developed. These actuators can be built lightweight in relatively small sizes. Since these actuators are small and light, a large number of these actuators can be used on the lifting surface so that any desired lifting surface deformation shape can be commanded for any flight mission.

To operate these solid state actuators with minimum power, there is a need to determine appropriate actuator locations and power ratings of the individual actuators. This report discusses a mathematical approach based on optimal control theory. Aircraft performance goals, such as pitch, roll and yaw rates, are used as the target quantities (constraints), while actuator power rating is taken as the objective function of

the design problem. Detailed discussions of synergetic design methodology, including the balancing of the aircraft, are presented in References 5 through 10.

2. ANALYTICAL MODELING OF AIRCRAFT DYNAMICS

2.1 Overview

The main objective of this study is to develop an analytical algorithm which helps to select the placement of actuators and their power ratings, so that desired flight load conditions and aircraft angular rates (pitch, roll and yaw) can be achieved with reduced actuator weight and minimum power. A general approach is used to develop a mathematical algorithm so that more complex maneuver performance requirements and structural design requirements can be included at a later time. Two mathematical models are presented, one based on the modal approach and the other using reduced structural degrees of freedom generally known as the ASET degrees of freedom. The modal approach is convenient to conduct some trade studies to assess system characteristics, but it is not a desirable model for the study of flight dynamics since the deformation of the wing caused by an actuator cannot accurately be represented by the linear combination of modal functions. Hence, a brief discussion of the ASET approach is also described.

2.2 Aircraft Dynamics using Modal Coordinate System

The equations of motion of maneuvering flexible aircraft can be written as:

$$Kr + C\dot{r} + M\ddot{r} + QT^T A_S \alpha + QT^T A_u(\kappa) r_a + F_u u + F_b = 0 \qquad (2\text{-}1)$$

where:

α = A vector of angle of attack at aerodynamic panels

A_S = Steady aerodynamic Influence Coefficients (AIC) matrix with respect to aerodynamic panels

F_u = Nodal forces generated from the actuator elements

K = Structural stiffness matrix in structural degrees of freedom (DOF)

M = Inertia matrix

r_a = A displacement vector at aero panel centers

r = A displacement vector at structural dof

T = A transformation matrix relating structural dof to aerodynamic dof

u = Vector of actuator stimuli (input in volt)

A_u = Incremental Unsteady aerodynamic influence coefficient matrix for

F_b = A body force vector due to gravitational and centripetal accelerations

Q = $\frac{1}{2}\rho V^2$ dynamic pressure

C = A damping matrix

κ = $\frac{\omega l}{V}$ reduced frequency, $\kappa > 0$

The displacement vector, **r**, can be expressed as a linear combination of rigid body modes and vibration modes. Thus, we have:

$$r = [\psi_r \psi_e] \begin{Bmatrix} \eta_r \\ \eta_e \end{Bmatrix} = [\psi]\eta \tag{2-2a}$$

$$r_a = T^T r = T^T \psi \eta = \psi_a \eta \tag{2-2b}$$

where:

ψ_r = A matrix of rigid body modes such as plunge (Z), sideslip (Y), pitch (θ), roll (ϕ), and yaw (ψ). The control surface rotation modes may also be adjoined to represent conventional aerodynamic effectors if desired

ψ_e = Matrix of vibration modes (including symmetric and antisymmetric components)

ψ_a = Transformation matrix in aero dof

η = $\{\eta_r, \eta_e\}$ a vector of generalized coordinates,

The subscript 'r' denotes rigid body modes, while 'e' denotes the elastic vibration modes.

Conventional aircraft use control surfaces to perform maneuvers. The vibration modal vectors may include rigid body deflection of the conventional control surfaces.

The angle of attack (incidence) at the center of each aerodynamic panel is given by:

$$\alpha = T\frac{\dot{r}}{V} = \frac{1}{V}T[\frac{\partial r}{\partial t} + U.\nabla r] = \frac{1}{V}T[\psi\dot{\eta} + u\frac{\partial \psi}{\partial x}\eta] \tag{2-3a}$$

or:

$$\alpha = \overline{\psi}\dot{\eta} + \psi_X \eta \tag{2-3b}$$

where:

$$\overline{\psi} = \frac{1}{V}T\psi, \tag{2-3c}$$

$$\psi_X = T\frac{\partial \psi}{\partial X} \tag{2-3d}$$

and:

V = is the free stream velocity

u = is the chord-wise component of V

η_r = $\{Z, Y, \phi, \theta, \psi, \delta_p, \delta_q, \delta_r\}$ is a vector of generalized rigid body coordinates

$\dot{\eta}_r$ = $\{\dot{Z}, \dot{Y}, p, q, r, \dot{\delta}_q, \dot{\delta}_p, \dot{\delta}_r\}$, is the corresponding velocity vector in rigid body motion

The control surface rotations are denoted by δ. The rigid body motion in the flight direction (x) has been omitted since the computation of drag is not accurate in the linear aerodynamic methods. Should accurate drag computation tools be available, then all six degrees of freedom in rigid body motion must be included in the analytical model.

From equation (2-3b), the rigid body angle of incidence and sideslip are given by:

$$\alpha_i = \theta - \frac{\dot{Z}}{V} \tag{2-4a}$$

$$\beta_i = -\frac{\dot{Y}}{V} \tag{2-4b}$$

Substituting equations (2-2a) and (2-3b) in (2-1), and pre-multiplying by ψ^T, one can rewrite the equations of motion in terms of the generalized coordinates, η:

$$\overline{K}\eta + \overline{C}\dot{\eta} + \overline{M}\ddot{\eta} + Q\overline{A}_{s1}\eta + Q\overline{A}_{s2}\dot{\eta} + Q\overline{A}_u(\kappa)\eta + \overline{F}_u u + \overline{F}_b = 0 \quad (2\text{-}5)$$

in which the generalized matrices are denoted by an overbar symbol.

We note that the air loads due to oscillatory motion are expressed in the frequency domain. Hence, there is a need to transform the air loads from the frequency domain to the time domain. The unsteady aerodynamic matrix, A_u can be expressed in terms of a truncated series as:

$$\overline{A}_u(\kappa) = A_0 + sA_1 + s^2 A_2 + (\frac{s}{\beta + s})A_3 \quad (2\text{-}6)$$

where:

$$s = i(\frac{l}{V})\omega = i\kappa \quad (2\text{-}7)$$

and β is the pole of the aerodynamic lag term.

Using equation (2-6) in (2-5), the dynamics of the aircraft reduces to:

$$K'\eta + C'\dot{\eta} + M'\ddot{\eta} + QA_3 X_a + F_u u + F_b = 0 \quad (2\text{-}8)$$

where:

$$K' = \overline{K} + Q\overline{A}_{s1} + QA_0 \quad (2\text{-}9)$$

$$C' = \overline{C} + Q\overline{A}_{s2} + Q(\frac{l}{V})A_1 \quad (2\text{-}10)$$

$$M' = \overline{M} + Q(\frac{l}{V})^2 A_2 \quad (2\text{-}11)$$

And the aerodynamic lag coordinate is given by:

$$X_a = \frac{s}{\beta + s}\eta \quad (2\text{-}12)$$

2.2.1 State Space Formulation

The second order differential equation (2-8) can be rewritten in terms of the first order one as shown:

$$\dot{X} + AX + Bu + F_b = 0 \tag{2-13}$$

Where state vectors are given by:

$$X = \begin{Bmatrix} \eta \\ \dot{\eta} \\ X_a \end{Bmatrix}, \tag{2-14}$$

$$\dot{X} = \begin{Bmatrix} \dot{\eta} \\ \ddot{\eta} \\ \dot{X}_a \end{Bmatrix} \equiv, \tag{2-15}$$

and state matrices are defined as:

$$A = \begin{bmatrix} 0 & -I & 0 \\ M^{-1}K' & M^{-1}C' & QM^{-1}A_3 \\ 0 & -I & (\frac{V}{l})\beta I \end{bmatrix}, \tag{2-16}$$

$$B = \begin{bmatrix} 0 \\ M^{-1}\overline{F}_u \\ 0 \end{bmatrix}, \tag{2-17}$$

$$F_b = \begin{bmatrix} 0 \\ M^{-1}\overline{F}_b \\ 0 \end{bmatrix} \tag{2-18}$$

in which I denotes a unit matrix.

Equation (2-13) represents a general formulation of aircraft dynamics. At the low end of the frequency spectrum it denotes aircraft flight maneuver problems, while at the higher end of the frequency spectrum it represents an aeroservoelastic environment. In subsequent sections the optimal control theory is described to address various types of problems such as:

- Flight dynamics and flight control
- Flutter envelop prediction and flutter suppression
- Transient response due to gust encounter and buffeting

2.2.2 Pade Approximation of Unsteady Aerodynamic Matrix

Let the incremental data be given by:

$$A_u(\kappa) = A(\kappa) - A(0) \tag{2-19}$$

Then the expansion can be written in the matrix notation:

$$[R][P] = \overline{A} \tag{2-20}$$

where:

$$R = \begin{bmatrix} I & 0 & -\kappa_1^2 I & \dfrac{\kappa_1^2}{\beta^2 + \kappa_1^2} \\ 0 & I & 0 & \dfrac{\beta}{\beta^2 + \kappa_1^2} \\ I & 0 & -\kappa_2^2 I & \dfrac{\kappa_2^2}{\beta^2 + \kappa_2^2} \\ 0 & I & 0 & \dfrac{\beta}{\beta^2 + \kappa_2^2} \\ I & 0 & -\kappa_3^2 I & \dfrac{\kappa_3^2}{\beta^2 + \kappa_3^2} \\ 0 & I & 0 & \dfrac{\beta}{\beta^2 + \kappa_3^2} \end{bmatrix} \tag{2-21}$$

$$P = \begin{bmatrix} A_0 \\ A_1 \\ A_2 \\ A_3 \end{bmatrix} \tag{2-22}$$

$$\overline{A} = \begin{bmatrix} \overline{A}_{R1} \\ \overline{A}_{I1} \\ \overline{A}_{R2} \\ \overline{A}_{I2} \\ \overline{A}_{R3} \\ \overline{A}_{I3} \end{bmatrix} \tag{2-23}$$

For known values of $\overline{A}(\kappa)$ at a number of reduced frequencies, the AIC matrices, A_0 through A_3 can be computed from equation (2-20) by the method of least squares.

2.2.3 Optimal Control Design

For a given set of actuator input u, equation (2-13) can be solved for the response X using any known numerical integration method. However to perform flight maneuver at a desired flight load factor, N_z, the actuator input u will be computed by the method of optimal control theory such that the actuator power is minimum.

The Hamiltonian function of this problem can be stated as:

$$h = \frac{1}{2}\varepsilon^T Q\varepsilon + U(\xi) + \lambda^T (AX + B\xi + F_b) \tag{2-24}$$

where:

A, B, F_b = are defined in equation (2-13)

ξ = u a vector of control variables

ε = a vector of constraint function

Q = a weighting matrix

λ = A vector of Lagrangian coefficients

The constraints can be expressed in several forms. In terms of state variables one can write:

$$\varepsilon = (X_d - X) = 0 \tag{2-25a}$$

Where, in steady symmetric pull-up maneuver at a load factor, N_{ZT}, the required constraint is:

$$\varepsilon_{\bar{q}} = \bar{q}_T - \bar{q} \tag{2-25b}$$

From the second row of equation (2-13) the nondimensional pitch rate is given by:

$$\bar{q} = -B_2\xi - f_{2b} \tag{2-25c}$$

and the target pitch rate is:

$$q_T = \frac{(N_{ZT} - 1)g}{V_0} \tag{2-25d}$$

Constraint on actuator strain is given in the following expressions. Let ε_a and ε be the allowable strain in the actuator material and the actual strain in the actuator when commanded. Then the difference between the allowable strain ε_a, and the actual strain in the actuator must be positive:

$$\Delta\varepsilon = \varepsilon_a - \varepsilon = \varepsilon_a - c\xi > 0 \qquad \text{(2-26a)}$$

in which c is a constant relating the actuator strain to the stimuli (electrical potential in volts).

The constraints based on aeroelastic stability criteria, using Lyapunov's direct method, may be written as:

$$\varepsilon(k) = \varepsilon_V - V > 0 \qquad \text{(2-26b)}$$

$$\varepsilon = \varepsilon_{\dot{V}} - \dot{V} < 0 \qquad \text{(2-26c)}$$

where V and $\dot{V}$ denote Lyapunov energy function and its rate of change in time,

in which ε_V and $\varepsilon_{\dot{V}}$ are prescribed constants.

The second term in the Hamiltonian function, eqn.(2-24), represents an objective function based on the strain energy in the actuator elements which is given by:

$$U(\xi) = \frac{1}{2}(c\xi)^T EAL(c\xi) = \frac{1}{2}\xi^T R\xi \qquad \text{(2-27a)}$$

where:

E = Young's modulus of the actuator material

A = cross sectional area of the actuator stack

L = length of the actuator

The weighting coefficient R is given by:

$$R = c^2 EAL \qquad \text{(2-27b)}$$

The main purpose of this objective function is to minimize the power input so that the actuator is not overly strained beyond its elastic limit. Likewise, stress or strain constraints based on primary structural members may also be included.

The constraint functions in general can be expressed as:

$$\varepsilon = \varepsilon_0 + \frac{\partial \varepsilon}{\partial X} X + \frac{\partial \varepsilon}{\partial \xi} \xi \tag{2-28a}$$

For symmetric pull-up in steady maneuver we have:

$$\frac{\partial \varepsilon}{\partial X} = 0 \tag{2-28b}$$

for all elements of X ,

and for the control variables, from second row of matrix B, the derivatives are given by:

$$\frac{\partial \varepsilon_{\bar{q}}}{\partial \xi} = B_2 \tag{2-28c}$$

and:

$$\frac{\partial \Delta \varepsilon_i}{\partial \xi_i} = c_{ii} \tag{2-28c}$$

Additional objective functions such as structural weight and aerodynamic figures of merit, may also be included in the objective function U .

2.2.4 Hamiltonian Equations of Motion

Differentiating the Hamiltonian function, h (equation 2-24), with respect to X , ξ (=u), and λ, and using the principle of optimal control theory, we obtain the following two-point boundary value problem:

$$\begin{Bmatrix} \dot{X} \\ \dot{\lambda} \end{Bmatrix} = \begin{bmatrix} h_{11} & h_{12} \\ h_{21} & h_{22} \end{bmatrix} \begin{Bmatrix} X \\ \lambda \end{Bmatrix} + \begin{Bmatrix} F_1 \\ F_2 \end{Bmatrix} = [H] \begin{Bmatrix} X \\ \lambda \end{Bmatrix} + \begin{Bmatrix} F_1 \\ F_2 \end{Bmatrix} \tag{2-29}$$

together with the incremental control (design) input:

$$\xi = -\Re^{-1} [\varepsilon_{\xi X} X + B^T \lambda + \varepsilon_{\xi 0}] \tag{2-30}$$

in which:

$$\Re = [R_i + \varepsilon_\xi^T Q \varepsilon_\xi] \tag{2-31}$$

The elements of the Hamiltonian matrix, H, in equation (2-29) are given by:

$$h_{11} = A - B\Re^{-1}\varepsilon_{\xi X} \tag{2-32}$$

$$h_{12} = -B\Re^{-1}B^T \tag{2-33}$$

$$h_{21} = -\varepsilon_{XX} + \varepsilon_{X\xi}\Re^{-1}\varepsilon_{\xi X} \tag{2-34}$$

$$h_{22} = -h_{11}^T \tag{2-35}$$

$$F_1 = F_b - B\Re^{-1}\varepsilon_{\xi 0} \tag{2-36}$$

$$F_2 = -\varepsilon_{X0} + \varepsilon_{X\xi}\Re^{-1}\varepsilon_{\xi 0} \tag{2-37}$$

The following definitions are used:

$$\varepsilon_{ij} = \varepsilon_i^T Q \varepsilon_j \qquad i = X,\xi \text{ and } j = X,\xi \tag{2-38}$$

$$\varepsilon_{i0} = \varepsilon_i^T Q \varepsilon_0 \qquad i = X,\xi \tag{2-39}$$

2.2.5 Solution to Hamiltonian Equations of Motion

The solution of the two-point boundary value problem stated in equation (2-29) can be written as,

$$\begin{Bmatrix} X(t_f) \\ \lambda(t_f) \end{Bmatrix} = \Phi(t_f,t)\begin{Bmatrix} X(t) \\ \lambda(t) \end{Bmatrix} + \int_t^{t_f} \Phi(t_f,\tau)\begin{Bmatrix} F_1(\tau) \\ F_2(\tau) \end{Bmatrix} d\tau \tag{2-39a}$$

where t_f denotes the final time frame, and Φ denotes the transition matrix.

The transition matrix can be computed as follows.

Let χ and χ' be right and left eigenvectors of the Hamiltonian matrix H, and Λ is a diagonal matrix of corresponding eigenroots. Then the transition matrix is given by:

$$\Phi(t_f,t) = \chi \exp(\Lambda(t_f - t))\chi' = e^{H(t_f - t)} \tag{2-39b}$$

The known end conditions are:

$$X(t) = X(t_0) \tag{2-40}$$

at $t = t_0$, the initial condition, while at the terminal condition:

$$\lambda(t_f) = 0 \tag{2-41}$$

Rewriting equation (2-39a) in matrix notation and using equations (2-40) and (2-41), one obtains:

$$\begin{Bmatrix} X(t_f) \\ \lambda(t_f) \end{Bmatrix} = \begin{bmatrix} \Phi_{11} & \Phi_{12} \\ \Phi_{21} & \Phi_{22} \end{bmatrix} \begin{Bmatrix} X(t) \\ \lambda(t) \end{Bmatrix} + \begin{Bmatrix} f_1(t) \\ f_2(t) \end{Bmatrix} \tag{2-42}$$

Multiplying equation (2-42) by the inverse of Φ and rearranging we obtain:

$$\begin{Bmatrix} X(t) \\ \lambda(t) \end{Bmatrix} = \begin{bmatrix} \Psi_{11} & \Psi_{12} \\ \Psi_{21} & \Psi_{22} \end{bmatrix} \begin{Bmatrix} X(t_f) \\ \lambda(t_f) \end{Bmatrix} - \begin{Bmatrix} \bar{f}_1(t) \\ \bar{f}_2(t) \end{Bmatrix} \tag{2-43}$$

At $t = 0$, we have:

$$X(t) = X(0)$$

and at $t = t_f$, we have:

$$\lambda(t_f) = 0$$

Thus, we get:

$$X(t_f) = [\Psi_{11}]^{-1}\{X(t) + \bar{f}_1\} \tag{2-44}$$

and the Lagrangian coefficient vector is given by:

$$\lambda(t) = \Psi_{21}\Psi_{11}^{-1}\{X(t)\} + \bar{f}_1\} - \bar{f}_2 \tag{2-45}$$

or:

$$\lambda(t) = \mathrm{P}(t)X(t) + s(t) \tag{2-46}$$

in which the Riccati matrix is denoted by:

$$\mathrm{P}(t) = \Psi_{21}\Psi_{11}^{-1} \tag{2-47}$$

Finally the control law is given by:

$$\xi(t) = -\Re^{-1}[[\varepsilon_{\xi X} + B^T \mathrm{P}]X(t) + B^T s(t) + \varepsilon_{\xi 0}] \tag{2-48}$$

2.2.6 *Alternate Riccati Matrix Solution*

Differentiating equation (2-46) with respect to time we obtain:

$$\dot{\lambda} = \dot{K}X + K\dot{X} + \dot{s} \tag{2-49}$$

Next, eliminating $\dot{\lambda}$ and $\dot{X}$, using equation (2-29), we obtain the following Riccati matrix equation:

$$\dot{K} + Kh_{11} - h_{22}K + Kh_{12}K - h_{21} = 0 \tag{2-50a}$$

together with:

$$\dot{s} + (Kh_{12} - h_{22})s + KF_1 - F_2 = 0 \tag{2-50b}$$

Since the initial conditions are not known for the elements of the Riccati matrix P the solution must be derived from the terminal conditions. If the coefficient matrix, h_{ij}, are constant, the solutions of P at various time intervals may be computed and stored which can be used in the aeroelastic analysis. Otherwise, the solution given by equation (2-47) is reasonably valid for a regulator problem.

2.2.7 *Closed Loop System*

We set the feedback control input:

$$u = \xi(t) = -\Re^{-1}[[\varepsilon_{\xi X} + B^T K]X(t) + B^T s(t) + \varepsilon_{\xi 0}] \tag{2-51}$$

and substituting in equation (2-13) we obtain the closed loop system:

$$\dot{X} = \overline{\mathrm{A}}X + \Im \tag{2-52}$$

where:

$$\overline{\mathrm{A}} = A - B\Re^{-1}B^T K - B\Re^{-1}\varepsilon_{\xi X} \tag{2-53}$$

$$\Im = F_b - B\Re^{-1}B^T s(t) - B\Re^{-1}\varepsilon_{\xi 0} \tag{2-54}$$

The eigenvalues of the closed system $\overline{\mathrm{A}}$ are stable, assuring the aircraft to be dynamically stable. However, appropriate gain matrix coefficients, Q, must be selected so that any unstable roots that lie in the right half of Nyquist's plane move to the left-half, the stable region. Lyapunov proposed a robust stability criterion of a nonlinear system. A brief outline is presented next.

2.2.8 Lyapunov Stability Criteria

A. M. Lyapunov (also written as Liapunov) proposed a robust stability criteria of nonlinear systems in 1892. This was practically ignored for many years. However, a French translation of his work appeared in 1907. Again it was forgotten for nearly a half-century. Due to a compelling need to establish the state of stability of nonlinear systems, engineers and scientists began recognizing the merits of the Lyapunov's stability criteria. Consequently, a German translation appeared in 1954 and an English translation in 1961.

A Lyapunov stability criterion primarily deals with the energy and rate of energy dissipation of a system. Hence, it is valid for linear as well as nonlinear systems. There are several ways to formulate Lyapunov's criteria. The stability criteria proposed here is well suited for complex and multidisciplinary systems.

Let the energy function be given by:

$$V(t) = \int_t^{\infty} X^T P X d\tau \quad >0 \tag{2-55}$$

in which P is a positive definite Riccati matrix solution of a closed loop system defined equation (2-52). The corresponding Riccati matrix equation is given by:

$$\dot{P} + \overline{\mathrm{A}}^T P + P\overline{\mathrm{A}}^T = -Q \tag{2-56}$$

Next we compute the rate of change V by finite difference:

$$\dot{V} = \frac{V(X,t_n) - V(X,t_{n-1})}{\Delta t} \tag{2-57}$$

A system is stable if for every finite time t:

$$V > 0 \tag{2-58}$$

and:

$$\dot{V} < 0 \tag{2-59}$$

These two Lyapunov stability criteria can be expressed in a single statement:

$$\varepsilon_L = V * \dot{V} < 0 \tag{2-60}$$

This concludes the generalized mathematical discussion of the dynamics of flexible aircraft. Next we will present some applications in steady maneuver cases.

2.2.9 Steady Symmetric Maneuver

Since we are interested in steady maneuver, the acceleration term in equation (2-13) is set to zero. In addition unsteady aerodynamic loads are not required in this study. Hence, the governing equation reduces to,

$$\eta + [\overline{\mathrm{K}} + Q\mathrm{A}]^{-1}[\Im u + f_b] = A\eta + Bu + \bar{f}_b = 0 \tag{2-61}$$

where the state vector and matrices are given by:

$$A = I \tag{2-62a}$$

$$\mathrm{B} = [\overline{\mathrm{K}} + Q\overline{\mathrm{A}}_s]^{-1}[F_u] \tag{2-62b}$$

$$\bar{f}_b = [\overline{\mathrm{K}} + Q\overline{\mathrm{A}}_s]^{-1}[f_b] \tag{2-62c}$$

$$\eta = \begin{Bmatrix} \alpha \\ \bar{q} \\ \eta_e \end{Bmatrix} \tag{2-62d}$$

in which the flight angle of attack is given by equation (2-4a). The inversion indicated in equations 2-62b and 2-62c must be performed with caution, since the elements of structural stiffness and aerodynamic matrices may be two to three order of magnitude different.

The expression for the actuator input in the case of steady maneuver, reduces to a very simple form. This can be derived, alternatively, from the Newton's method as discussed next.

2.2.10 Newton's Method

The Hamiltonian function will be replaced by quadratic functions without using the Lagrangian coefficients λ (see eqn. 2-24), i.e.

$$h = \frac{1}{2}\varepsilon^T Q_X \varepsilon + U(\xi) + (AX + B\xi + \bar{f}_b)^T (AX + B\xi + \bar{f}_b) \tag{2-63}$$

The resulting equilibrium equation takes the following form:

$$\begin{bmatrix} I & B \\ B^T & \Re \end{bmatrix} \begin{Bmatrix} X \\ \xi \end{Bmatrix} = \begin{Bmatrix} -\bar{f}_b \\ -f_2 \end{Bmatrix} \tag{2-64}$$

where:

$$\Re = R + B^T B + B_2^T Q(2) B_2 + c^2 Q \tag{2-65}$$

$$f_2 = B^T f_b - cQ + B_2^T Q(2)(\bar{q}_T + \bar{f}_b(2)) \tag{2-66}$$

This approach has some merit over the Lagrangian in that the Hamiltonian function is strictly a convex function leading to an absolute minimum value of the Hamiltonian. However, there may be many solutions. Valid ones are admitted when all constraints are satisfied. In the present examples both methods produced identical results.

2.2.11 Steady Roll Maneuver

Steady roll maneuvers are performed at 1g load factor. Hence, the external body forces vector:

$$\bar{f}_b = 0 \tag{2-67}$$

and the equilibrium equation reduces to:

$$\begin{Bmatrix} \bar{p} \\ \eta_e \end{Bmatrix} = -\left[\overline{\mathrm{K}} + Q\overline{\mathrm{A}}\right]^{-1} \Im \xi = -\mathrm{B}\xi \tag{2-68a}$$

or:

$$A\eta + B\xi = 0 \tag{2-68b}$$

in which the nondimensional roll rate is given by:

$$\bar{p} = \left(\frac{pl}{V_0}\right) \tag{2-69}$$

In this case antisymmetric vibration modes including one rigid body roll mode will be selected. Then the generalized coordinate vector is given by:

$$\eta = \begin{Bmatrix} \bar{p} \\ \eta_e \end{Bmatrix} \tag{2-70}$$

The corresponding constraint is given by:

$$\varepsilon = \bar{p}_T - \bar{p} = \bar{p}_T - \mathrm{B}_1 \xi = 0 \tag{2-71}$$

2.3 Aircraft Dynamics using Reduced Structural Degrees of Freedom

The equations of motion of an elastic aircraft can be written as:

$$Kr + Ma + Q\Psi^T A\alpha + F_g + F_u u = 0 \qquad (3\text{-}1)$$

where:

K = Structural stiffness matrix in structural (ASET) degrees of freedom

M = Mass matrix consistent with K

A = AIC matrix in aerodynamic with respect to aero panels

Ψ = Transformation matrix relating structural dof to aerodynamic dof

a = Vector of accelerations in a moving coordinate system fixed to aircraft

α = Angle of attack at aero panels

F_g = Vector of gravity forces and engine thrust

F_u = Vector of nodal forces created by the solid state actuators

u = Vector of actuator stimuli (e.g. volt)

r = Displacement vector including rigid and elastic d.o.f.

The displacement vector can be expressed as a linear combination of rigid body modes and elastic degrees of freedom. Thus, we have:

$$r = \begin{bmatrix} I_e & T_{rs} \\ 0 & \end{bmatrix} \begin{Bmatrix} r_e \\ \rho \end{Bmatrix} = [T]\hat{r} \qquad (3\text{-}2a)$$

where:

I_e = A unit matrix

T_{rs} = A matrix of rigid body modes at structural nodes

T = A transformation matrix defined by equation (3-2a)

r_e = $\{u \quad v \quad w\}$ a vector of elastic displacements measured with respect to the statically determinant supports

In roll and symmetric maneuvers only w component need be selected at each ASET point, whereas in banked turn or rolling pullout maneuvers u, v, and w components must be selected.

$$\hat{r} = \begin{Bmatrix} r_e \\ \rho \end{Bmatrix} \tag{3-2b}$$

$$\rho = \{X_0, Y_0, Z_0, \phi, 6, \psi\} \tag{3-2c}$$

is a rigid body vector consisting of three displacements and three rotations of the center of mass of the aircraft. The corresponding velocities are given by:

$$\dot{\rho} = \{U_0, V_0, W_0, p, q, r\} \tag{3-2d}$$

The trim angle of attack and sideslip angle are given by:

$$\alpha_0 = \frac{W_0}{U_0}, \beta_0 = \frac{V_0}{U_0} \tag{3-3}$$

The angle of attack α is given by:

$$\alpha = \psi \frac{\dot{r}}{V} = \psi \frac{1}{V}[\frac{\bar{o}r}{\bar{o}t} + U.\nabla r] = \psi[\frac{1}{V}[\psi_r \dot{\rho} + u \frac{\bar{o}r_e}{\bar{o}x}]] \tag{3-4}$$

or:

$$\alpha = \overline{\psi}_x \hat{r} + \frac{1}{V} \overline{\psi}_r \dot{\hat{r}} \tag{3-5a}$$

in which slope transformation matrix from structure to aero grids:

$$\overline{\psi}_x = [\psi_{xa} \quad 0] \tag{3-5b}$$

and the rigid body modal matrix at aero grids:

$$\overline{\psi}_r = [0 \quad \psi_{ra}] \tag{3-5c}$$

The first term in equation (3-4) denotes the slope due to elastic deformation, while the second part represents the angle of attack due to rigid body velocities, with V as the free stream velocity.

The acceleration vector following Reference 5 can be written as:

$$a = T\ddot{\hat{r}} + T_c \dot{\hat{r}} \tag{3-6}$$

in which:

$$T_c = \Omega \begin{bmatrix} I_e & T_{rs} \\ 0 & \end{bmatrix} \tag{3-7}$$

$\Omega = \{\omega, \ldots\ldots \omega\}$ is a 3n*3n superdiagonal matrix with constant ω (3-8a)

with:

$$\omega = \begin{bmatrix} 0 & -r & q \\ r & 0 & -p \\ -q & p & 0 \end{bmatrix} \tag{3-8b}$$

p, q and r are the rigid body angular velocities of the aircraft in the body fixed coordinate system.

The first term in equation (3-6) represents accelerations due to translation and angular motions, while the second term denote the centripetal acceleration of a maneuvering aircraft. The coriolis acceleration terms are omitted being small in an inertial frame fixed to a flat surface on the earth.

The external force vector F_g, is given by:

$$F_g = Ma_g + \vec{T} \tag{3-9a}$$

in which the gravitational acceleration vector is given by:

$$a_g = \begin{Bmatrix} -Sin\theta Cos\phi \\ Sin\phi \\ Cos\theta Cos\phi \end{Bmatrix} \tag{3-9b}$$

$$\vec{T} = \begin{Bmatrix} T_x \\ 0 \\ 0 \end{Bmatrix} \quad \text{a thrust vector} \tag{3-9c}$$

Pitch angle:

$$\theta = \alpha + \gamma \tag{3-9d}$$

Angle of attack:

$$\alpha = \frac{w}{V_0} \tag{3-9e}$$

With these definitions, equation (3-1), after premultiplying by the transformation matrix, T, reduces to:

$$\overline{K}\hat{r} + \overline{M}\ddot{\hat{r}} + \overline{A}\dot{\hat{r}} + \overline{F}_g + \overline{F}_u u = 0 \tag{3-10}$$

where:

$$\overline{K} = T^T K T + Q T^T \psi^T A \psi_X \tag{3-11}$$

$$\overline{M} = T^T M T \tag{3-12}$$

$$\overline{A} = T^T M T_c + Q T^T \psi^T A \psi_r \tag{3-13}$$

$$\overline{F}_g = T^T F_g \tag{3-14}$$

$$\overline{F}_u = T^T F_u \tag{3-15}$$

The flight dynamics defined by equation (3-10) can be rewritten in terms of the state space coordinate vector, X;

$$\dot{X} = AX + Bu + f_g \tag{3-16}$$

where:

$$X = \begin{Bmatrix} \hat{r} \\ \dot{\hat{r}} \end{Bmatrix} \tag{3-17}$$

$$A = \begin{bmatrix} 0 & -I \\ -\overline{M}^{-1}\overline{K} & -\overline{M}^{-1}\overline{A} \end{bmatrix} \tag{3-18}$$

$$B = \begin{bmatrix} 0 \\ -\overline{M}^{-1}\overline{F}_u \end{bmatrix} \tag{3-19}$$

$$f_g = \begin{bmatrix} 0 \\ -\overline{M}^{-1}\overline{F}_g \end{bmatrix} \tag{3-20}$$

The solution to this problem can be found by means of the optimal control theory discussed next.

2.3.1 Transient Maneuver Analysis

Hamiltonian function can be stated as:

$$h = \frac{1}{2}\varepsilon^T Q\varepsilon + \frac{1}{2}u^T Ru + \lambda^T(\dot{x} - Ax - Bu - f_g) \tag{3-21}$$

where the first term represents a function of target errors, the second term denotes the actuator power, and the third term defines the aircraft dynamics. λ is a vector of Lagrangian coefficients.

The error vector, ε, may consist of several constraints such as the load factor, roll angle, angular velocities or accelerations. The weighting coefficient matrix is given by Q.

The constraint function may be classified as those based on state variables, X and the control variables, u. The corresponding weighting coefficients will be denoted by Q_X and Q_u.

A typical constraint function is given by:

$$\varepsilon_k = 1 - c_k\xi_k \tag{3-22a}$$

in which ξ denotes either X or u.

The angle of attack is given by:

$$\alpha = \frac{\dot{Z}_0}{V} \tag{3-22b}$$

and the sideslip angle is given by:

$$\beta = \frac{\dot{Y}_0}{V} \tag{3-22c}$$

2.3.2 Hamiltonian Equations of Motion

Differentiating the Hamiltonian function, h (equation 3-21), with respect to X, u, and λ, and using the principle of optimal control theory we obtain the following two point boundary value problem:

$$\begin{Bmatrix}\dot{X}\\ \dot{\lambda}\end{Bmatrix} = \begin{bmatrix}h_{11} & h_{12}\\ h_{21} & h_{22}\end{bmatrix}\begin{Bmatrix}X\\ \lambda\end{Bmatrix} + \begin{Bmatrix}F_1\\ F_2\end{Bmatrix} \tag{3-23}$$

together with the control input:

$$u = -\Re^{-1}[B^T \lambda - Q_u C_u] \tag{3-24}$$

in which:

$$\Re = R + Q_u c_u{}^2 \tag{3-25}$$

is a diagonal weighting matrix.

The elements of the Hamiltonian matrix in equation (3-23) are given by:

$$h_{11} = A \tag{3-26}$$

$$h_{12} = -B\Re^{-1}B^T \tag{3-27}$$

$$h_{21} = -Q_X c_X{}^2 \tag{3-28}$$

$$h_{22} = -h_{11}^T \tag{3-29}$$

$$F_1 = -[f_g + B\Re^{-1}\{Q_u c_u\}] \tag{3-30}$$

$$F_2 = Q_X c_X \tag{3-31}$$

The solution procedure involving two end conditions at different time intervals is somewhat more difficult, than the ordinary transient problems with known initial conditions. A brief account of the solution procedure with respect to the transient maneuver analysis using distributed solid state actuators will be presented next (see also Ref. 6).

2.3.3 Steady Maneuver Analysis

In the case of steady maneuver analysis, the acceleration terms, $\ddot{r}$, defined in equation (3-10) will be set to zero. In addition, the contributions from $\dot{r}_e$ and ρ can be omitted since they have zero or negligible effect on aerodynamic forces. Then the equilibrium equations can be simplified with the following definition for the state vector:

$$\hat{X} = \begin{Bmatrix} r_e \\ \dot{\rho} \end{Bmatrix} \tag{3-32}$$

The corresponding Hamiltonian function is:

$$h = \frac{1}{2}\varepsilon^T Q\varepsilon + \frac{1}{2}u^T Ru + \lambda^T (Ax + Bu + f_g) \tag{3-33}$$

with

$A = I$ a unit matrix

$$B = \left[\overline{K} + \overline{A}\right]^{-1} \overline{F}_u \tag{3-34}$$

$$f_g = \left[\overline{K} + \overline{A}\right]^{-1} \overline{F}_g \tag{3-35}$$

The Hamiltonian matrix is:

$$\begin{bmatrix} A & -\overline{B} \\ -\overline{D} & -A^T \end{bmatrix} \begin{Bmatrix} \hat{X} \\ \lambda \end{Bmatrix} = \begin{Bmatrix} \bar{f}_g \\ f_1 \end{Bmatrix} \tag{3-36}$$

$$\overline{B} = B\Re^{-1}B^T$$

$$\overline{D} = \left[Q_X c_X{}^2\right], \text{ a diagonal matrix} \tag{3-37}$$

$$\bar{f}_g = -[f_g + B\Re^{-1}\{Q_u c_u\}] \tag{3-38}$$

$$f_1 = \{Q_x c_x\} \tag{3-39}$$

Thus, we obtain the solution:

$$\begin{bmatrix} \hat{X} \\ \lambda \end{bmatrix} = \begin{bmatrix} C_{11} & C_{12} \\ C_{21} & C_{22} \end{bmatrix} \begin{Bmatrix} \bar{f}_g \\ f_1 \end{Bmatrix} \tag{3-40}$$

where:

$$\begin{aligned} C_{11} &= [I + \overline{BD}]^{-1} \\ C_{22} &= -[I + \overline{DB}]^{-1} \\ C_{12} &= \overline{B}C_{22} \\ C_{21} &= -\overline{D}C_{11} \end{aligned} \tag{3-41}$$

Thus, the actuator input for required maneuver is given by:

$$u = -\Re^{-1}[B^T\lambda - Q_u C_u] \tag{3-42}$$

2.4 Case 1: 1-g Roll

Given:

1. Roll rate $p_{require}$
2. Selected ASET displacement degrees of freedom w on the wing surface and u at the actuator end points.
3. Apply constraints on:
    - Roll rate
    - Displacements w and u
    - Strain in the actuator
    - Strains at wing root and mid section etc.

Solution:

1. Actuator input
2. Net load distributions, shear, bending and torsion
3. Deformed shape of the wing

2.5 Case 2: Pull-up or Push-over maneuver

Given:

1. Load Factor: N_Z
2. Required pitch Rate: $q_{required} = \frac{(N_Z - 1)g}{V}$
3. Roll rate: $p = 0$
4. Yaw rate: $r = 0$
5. Pitch angle: $\theta = \alpha + \gamma$
6. Angle of attack: $\alpha = \frac{w}{V_0}$

7. Climb angle: $\gamma = Sin^{-1}(\frac{T-D}{W})$

8. Selected ASET degrees of freedom u and w on the upper wing surface and u at the actuator end points.

9. Constraints on:

   - Pitch rate
   - Displacements
   - Strain in the actuator
   - Strains at wing root and mid section etc.

Where:

g = Gravitational acceleration inch/sec^2

V = Aircraft velocity in inch/sec

Solution:

1. Angle of attack and actuator input
2. Net load distributions, shear, bending and torsion
3. Deformed shape of the wing

2.6 Case 3: Banked turn with Glide

Given:

1. Bank angle ϕ and glide angle γ
2. Pitch angle: $\theta = \alpha + \gamma$
3. Angle of Attack: $\alpha = \frac{w}{V_0}$
4. Roll rate: $p = -(\frac{g}{V})\tan\phi Sin\gamma$

5. Pitch rate: $q = (\frac{g}{V}) \tan\phi Cos\gamma Sin\phi$

6. Yaw rate: $r = (\frac{g}{V}) \tan\phi Cos\gamma Cos\phi$

7. Selected ASET degrees of freedom u, v, and w on the wing surface and u at the actuator end points.

8. Constraints on:

   - Angular rates
   - Displacement w and u
   - Strain in the actuator
   - Strains at wing root and mid section etc.

Where:

g = Gravitational acceleration inch/sc^2

V = Aircraft velocity in inch/sec

3. COMPUTER PROGRAM IMPLEMENTATION WITH ASTROS

3.1 Outline of the Algorithm

The current implementation of the Smart Actuation system is a two step process, illustrated in Figure 3-1.

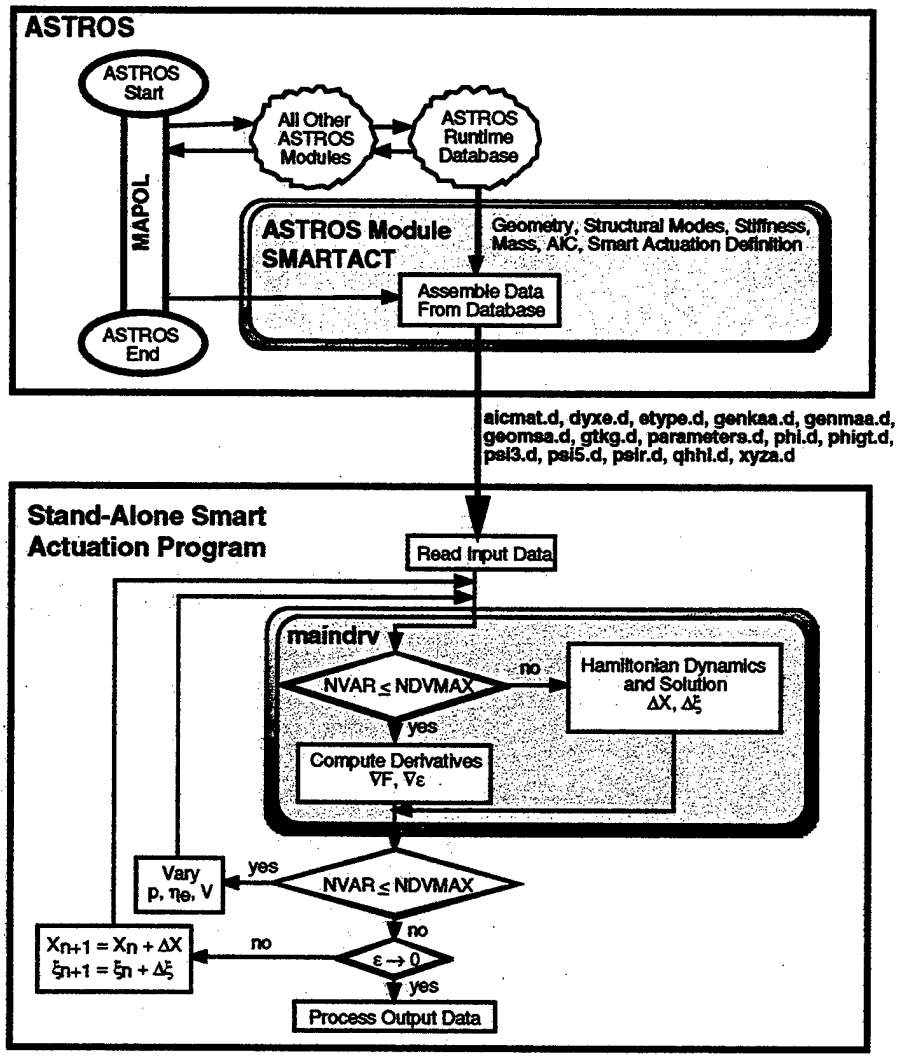

Figure 3-1. Overview of ASTROS/Smart Actuation System

3.1.1 Step One

In the first step, a special version of ASTROS VERSION 11 creates stiffness, mass, and aerodynamic matrices that are required in the Smart Actuation system computer program. Two additional bulk data entries, SACNTL and SAELIST, are required to define data that is specific to this process. These bulk data entries are described in subsequent sections. The following files are generated by ASTROS:

	Format	**Description**
aicmat.d	2000(1X,E12.5)	Matrix of aerodynamic influence coefficients.
dyxe.d	2000(1X,E12.5)	$\frac{\partial \psi_e}{\partial x}$: Transforms elastic modes to aerodynamic panels.
etype.d	A8	Element types
genkaa.d	2000(1X,E12.5)	Generalized stiffness matrix.
genmaa.d	2000(1X,E12.5)	Generalized mass matrix.
geomsa.d	2(I8,1X),3(1PE12.5,1X)	Steady aerodynamics geometry description: Column — Description 1 — External aerodynamic box ID 2 — Internal aerodynamic box ID 3 — X location of box centroid in basic coordinates 4 — Y location of box centroid in basic coordinates 5 — Z location of box centroid in basic coordinates
gtkg.d	2000(1X,E12.5)	ASTROS [GTKG] matrix.
parameters.d	FORTRAN 'Parameter'	Problem-dependent variable values which should be included in Kari Appa's Smart Actuation program.
phi.d	2000(1X,E12.5)	Matrix of mode shapes.
phigt.d	2000(1X,E12.5)	Transpose of ASTROS [PHIG] matrix.

psi3.d	2000(1X,E12.5)	Rigid body plunge mode matrix for aerodynamics model. This file will only be generated for runs with symmetric boundary conditions.
psi5.d	2000(1X,E12.5)	Rigid body pitch mode matrix for aerodynamics model. This file will only be generated for runs with symmetric boundary conditions.
psir.d	2000(1X,E12.5)	Rigid body roll mode matrix for aerodynamics model. This file will only be generated for runs with antisymmetric boundary conditions.
qhhl.d	1X,I8 1X,I8 2000(1X,E12.5) 2000(1X,1PD12.5)	Number of modes Number of reduced frequencies Reduced frequencies ASTROS [QHHL] matrix list of generalized unsteady aerodynamic coefficients. This file will only be output if a flutter analysis is performed in the same boundary condition as the SAERO and MODES analyses.
xyza.d	I8,14(1PE12.5)	Actuator element descriptions:

		Column	Description
		1	Element ID
		2	X Coordinate of grid 1 in the basic system
		3	Y Coordinate of grid 1 in the basic system
		4	Z Coordinate of grid 1 in the basic system
		5	X Coordinate of grid 2 in the basic system
		6	Y Coordinate of grid 2 in the basic system
		7	Z Coordinate of grid 2 in the basic system
		8	X Coordinate of grid 3 in the basic system
		9	Y Coordinate of grid 3 in the basic system
		10	Z Coordinate of grid 3 in the basic system
		11	X Coordinate of grid 4 in the basic system
		12	Y Coordinate of grid 4 in the basic system
		13	Z Coordinate of grid 4 in the basic system
		14	Young's Modulus
		15	Cross sectional area or membrane thickness

3.1.2 Step Two

The second step of the process is to run the Smart Actuation program. The data sets that were generated in Step One are used as inputs to the Smart Actuation program.

3.2 User's Guide

3.2.1 Overview

This section provides updates to the ASTROS VERSION 11 User's Manual. The sections that are affected are noted where appropriate.

3.2.2 MAPOL Engineering Modules

This section provides additional documentation to Section 2.4.2.1 of the ASTROS VERSION 11 User's Manual.

MODULE	TYPE	DESCRIPTION
SMARTACT	ENGINEERING	Compute and assemble data required for Smart Actuation calculations.

3.2.3 Bulk Data Descriptions

This section provides additional documentation to Section 4.7 of the ASTROS VERSION 11 User's Manual.

Input Data Entry **SACNTL**

Description: Defines control parameters to the Smart Actuation module.

Format and Example:

1	2	3	4	5	6	7	8	9	10
SACNTL	SID	ITRMAX	RMODES	EMODES	ERRTOL				
SACNTL	101	10	1	3	0.001				

Field	Contents
SID	Set identification number (Integer > 0)
ITRMAX	Maximum number of design iterations (Integer > 0)
RMODES	Set identification number of a **MODELIST** bulk data entry that is used to request the rigid body modes that are to be used for the Smart Actuation analysis (Integer)
EMODES	Set identification number of a **MODELIST** bulk data entry that is used to request the elastic modes that are to be used for the Smart Actuation analysis (Integer)
ERRTOL	Iteration convergence criteria (Real, Default = 0.001)

Input Data Entry **SAELIST**

Description: Defines the list of actuation elements to the Smart Actuation module.

Format and Example:

1	2	3	4	5	6	7	8	9	10
SAELIST	SID	ETYPE	EID1	EID2	EID3	EID4	EID5	EID6	CONT
CONT	EID7	EID8	-etc-						

SAELIST	1001	ROD	1001	1002	1003	1004			

Alternate Form:

1	2	3	4	5	6	7	8	9	10
SAELIST	SID	ETYPE	EID1	THRU	EID2				

Field	Contents

SID Set identification number. (Integer > 0)

ETYPE Character input identifying the element type (See Note 1). One of the following:

BAR	**SHEAR**
QDMEM1	**TRIA3**
QUAD4	**TRMEM**
ROD	

EIDi Element identification number (Integer > 0 or blank)

Remarks:

1. Currently, only the **ROD** element is supported by the Smart Actuation algorithm. All other element types are included here for future development.
2. **SID** is here for future implementations of the Smart Actuation system which may be more general.
3. If the alternate form is used, **EID2** must be greater than or equal to **EID1**.
4. Nonexistent elements may be referenced and will result in no error message.
5. Any number of continuations is allowed.

3.3 Programmer's Guide

3.3.1 Overview

This section provides updates to the ASTROS VERSION 11 Programmer's Manual. The sections that are affected are noted where appropriate.

3.3.2 Engineering Application Modules

This section provides additional documentation to Section 5 of the ASTROS VERSION 11 Programmer's Manual.

Engineering Application Module: **SMARTACT**

Entry Point: **SMARTACT**

Purpose:

To assemble and calculate data required for Smart Actuation analysis

MAPOL Calling Sequence:

CALL SMARTACT (BC, SACNTL, SAELIST, [PHIG(BC)], LAMBDA, BGPDT(BC), BEAMEST, QDMM1EST, QUAD4EST, RODEST, SHEAREST, TRIA3EST, TRMEMEST, [DYX], [GENKAA], [GENMAA], [AICMAT(MINDEX)], [AAICMAT(MINDEX)], TRIM, OGPWG, CASE, GEOMSA, [GTKG], MAT1, MODELIST, SUPORT, [MGG], [QHHLFL(BC,SUB)], MKAERO1, MKAERO2);

BC	Boundary condition number(Integer, Input)
SACNTL	Relation of smart actuation control parameters (Input)
SAELIST	Relation of smart actuation elements (Input)
[PHIG(BC)]	Matrix of global eigenvectors from real eigenanalysis (Input)
LAMBDA	Relation of real eigenvalue analysis results (Input)
BGPDT(BC)	Basic grid point definition table (Input)
BEAMEST	Relation summarizing the **CBAR** element (Input)
QDMM1EST	Relation summarizing the **CQDMEM1** element (Input)
QUAD4EST	Relation summarizing the **CQUAD4** element (Input)
RODEST	Relation summarizing the **CONROD** and **CROD** element (Input)
SHEAREST	Relation summarizing the **CSHEAR** element (Input)
TRIA3EST	Relation summarizing the **CTRIA3** element (Input)
TRMEMEST	Relation summarizing the **CTRMEM** element (Input)

[DYX]	Elastic modes splined to the aerodynamic model (Input)
[GENKAA]	Generalized stiffness (Input)
[GENMAA]	Generalized mass (Input)
[AICMAT(MINDEX)]	Symmetric aerodynamic influence coefficients (Input)
[AAICMAT(MINDEX)]	Antisymmetric aerodynamic influence coefficients (Input)
TRIM	Relation containing trim parameters (Input)
OGPWG	Relation containing data from the grid point weight generation computations (Input)
CASE	Relation containing the case parameters for each analysis within each boundary condition (Input)
GEOMSA	Relation containing data on the geometric location of the aerodynamic degrees of freedom (Input)
[GTKG]	Interpolation matrix relating the forces at the aerodynamic degrees of freedom to the forces at the global structural degree of freedom (Input)
MAT1	Relation containing material properties (Input)
MODELIST	Relation containing lists of normal modes (Input)
SUPORT	Relation containing supported degrees of freedom (Input)
[MGG]	Global mass matrix (Input)
[QHHLFL(BC,SUB)]	Matrix list of generalized unsteady aerodynamic coefficients (Input)
MKAERO1	Relation containing table of Mach numbers and reduced frequencies (Input)
MKAERO2	Relation containing Mach number and reduced frequency pairs (Input)

Application Calling Sequence:

None

Method:

First the **CASE** entries associated with **SAERO** and **SAERO2** subcases for the current boundary condition are read into memory. The control parameters from the **SACNTL** entries are then read. The number of normal modes is obtained by opening the **[PHIG]** matrix. The lists of normal modes are read from the **MODELIST** entries. Then the list of smart actuation elements is read from the **SAELIST** entries. The material properties are read from the **MAT1** entries. The Basic Grid Point Definition Table is read from the **BGPDT** relation. For each smart actuation element, the data in the associated ***EST** relation is read. The G-Set modes matrix is read, transposed, and reduced to the desired modes. The global mass matrix, **MGG**, is read. The **massv** vector is created by summing the rows of **MGG** and multiplying by the transpose of **PHIG**. The **DYX** matrix is read and reduced to the desired elastic modes. The **GTKG** interpolation matrix is read. The **PHI** matrix and **XYZA** matrices are assembled for the smart actuation elements. **PHI** describes, for each mode, the generalized behavior for each smart actuation element:

The **XYZA** matrix describes the smart actuation element connectivity. The generalized mass and stiffness matrices are read. The **AIC** matrix is read. The free stream velocity is read from the **TRIM** relation. The center of gravity is read from the **OGPWG** relation. The aerodynamic geometry is read in from the **GEOMSA** relation. The **SUPORT** relation is read to obtain information about the supported degrees of freedom. For antisymmetric boundary conditions, the rigid body aerodynamic roll mode matrix, **PSIR**, is assembled. For symmetric boundary conditions, the **PSI3** and **PSI5** rigid body plunge and pitch mode matrices are assembled. If a flutter analysis has been performed, the **QHHL** matrix list is read and reduced to the desired modes. The reduced frequencies are read. The data required for the smart actuation loop is now assembled.

Design Requirements:

None

Error Conditions:

None

3.3.3 Database Entity Descriptions

This section provides additional documentation to Section 9 of the ASTROS VERSION 11 Programmer's Manual.

Entity: **SACNTL**

Entity Type: Relation

Description: Contains control parameters for the Smart Actuation System.

Relation Attributes:

NAME	TYPE/KEY	DESCRIPTION
SID	Integer > 0	Set identification number
ITRMAX	Integer > 0	Maximum number of design iterations
RMODES	Integer	Set identification number of a **MODELIST** bulk data entry that is used to request the rigid body modes that are to be used for the Smart Actuation analysis
EMODES	Integer	Set identification number of a **MODELIST** bulk data entry that is used to request the elastic modes that are to be used for the Smart Actuation analysis
ERRTOL	REAL	Iteration convergence criteria

Created By: Module IFP

Entity: **SAELIST**

Entity Type: Relation

Description: Contains the list of smart actuation elements.

Relation Attributes:

NAME	TYPE/KEY	DESCRIPTION
SID	Integer > 0	Set identification number
ETYPE	Text (8)	Element Type. One of the following: **BAR** **QDMEM1** **QUAD4** **ROD** **SHEAR** **TRIA3** **TRMEM**
EID	Integer > 0	Element Identification Number

Created By: Module IFP

4. DISCUSSION OF RESULTS

4.1 Aerodynamic Effectors

To verify the accuracy of the algorithm discussed in previous sections, a simple wing planform, shown in Figure 4-1, was selected. Figure 4-2 shows the smoothly deformable trailing edge control surface mechanism used in this analysis. Five pairs of solid state actuators were used to deform the trailing edge control surface. The actuators either pull or push the stringers. Thus, a small amount of bending moment is applied to top and bottom skin surfaces so that the control surface can curl up or down according to the direction of the stimuli. In this model, ten actuators were used along the trailing of the wing.

An alternate actuation system using distributed actuators as the diagonal elements of the ribs in the tip section of the wing was also examined to determine the relative merits of the two configurations of aerodynamic effectors. Figure 4-3 shows the location of forty actuators. A number of performance analyses were conducted. The results are presented next.

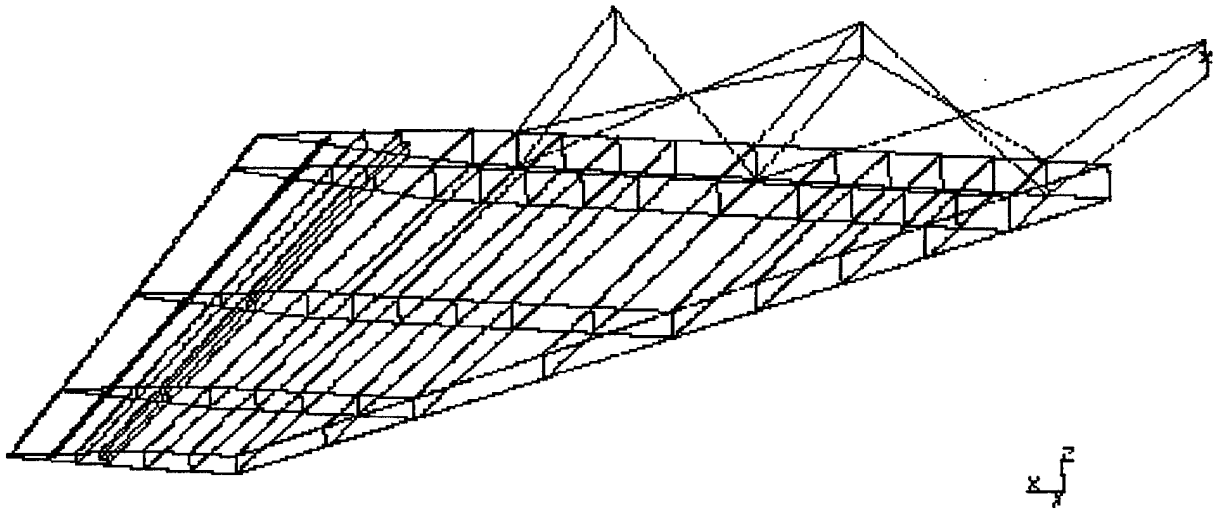

Figure 4-1 A low aspect ratio wing showing structural elements

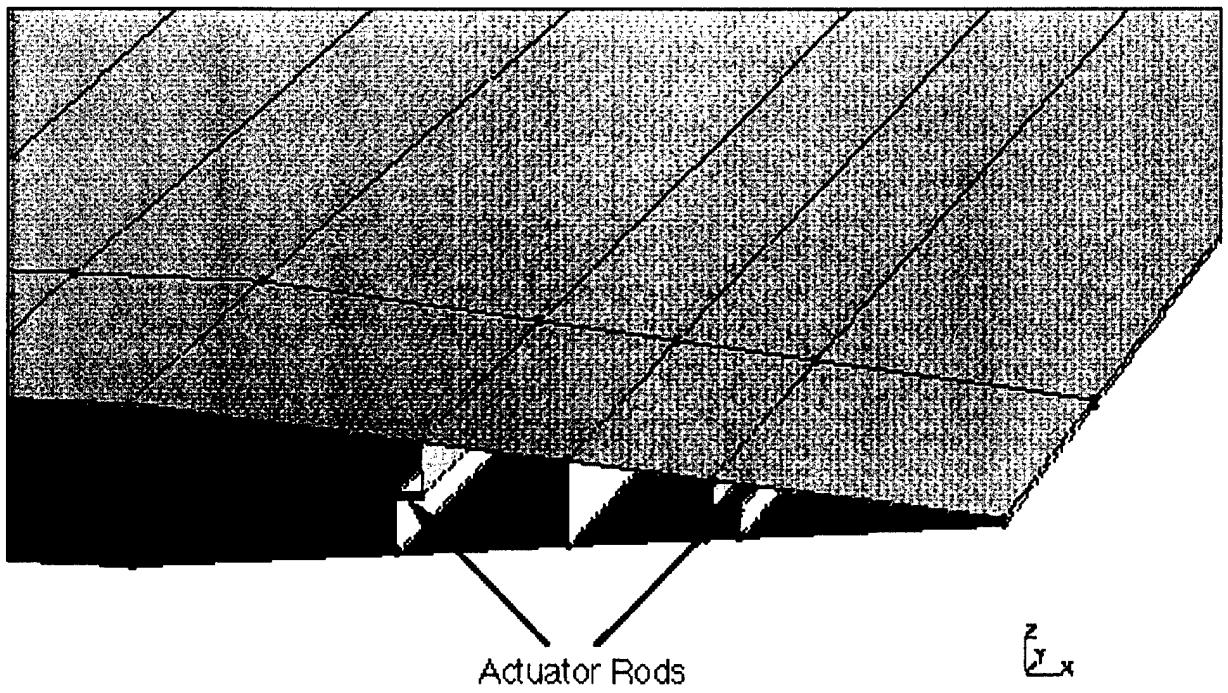

Figure 4-2 Trailing edge control surface showing solid state actuation mechanism

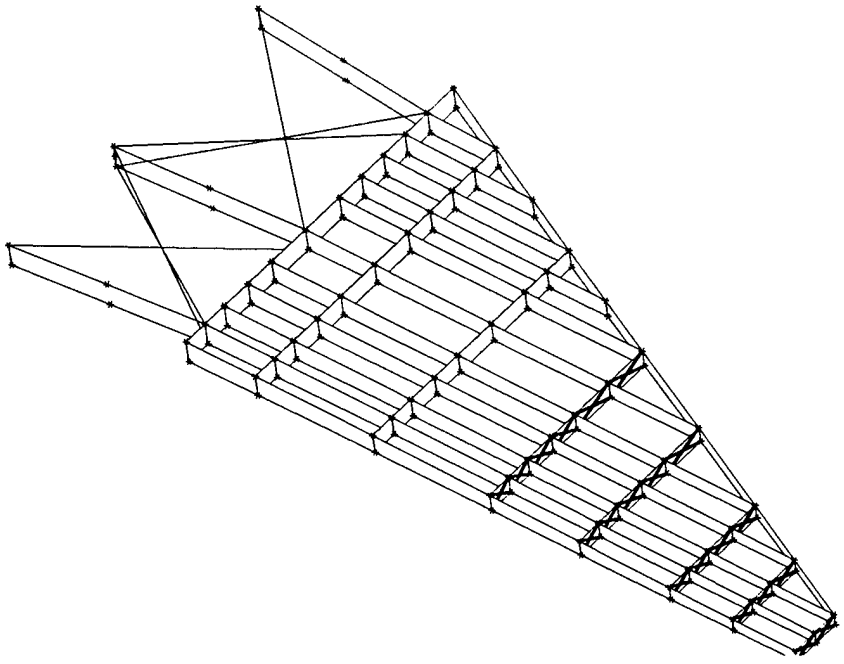

Figure 4-3 Diagonal Actuators located along ribs in the tip section of wing

4.2 Example 1: Steady Roll Maneuver

Altitude	Sea level
Mach Number	M = 0.5
Roll rate	p_T = 3.0 radians/sec
Number of actuators	10 along wing trailing edge
Objective function	Minimum total power required
Constraints	Target value of p_T , and strain allowable in the actuators

The deformed shape of the wing in 1.0 g roll maneuver is shown in Figure 4-4.

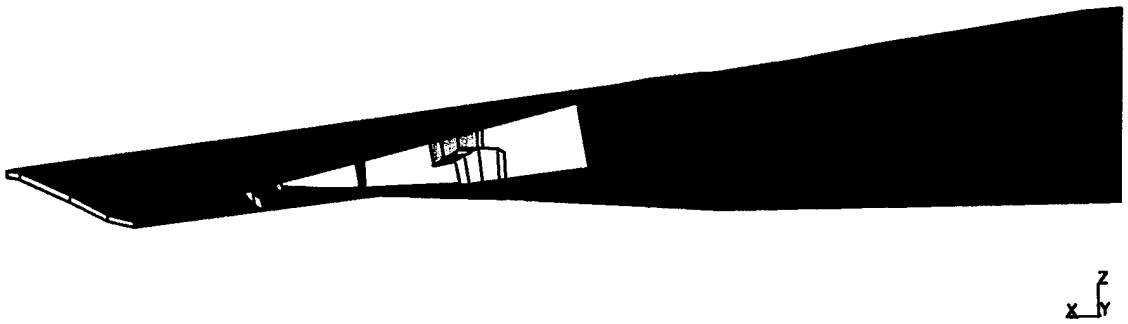

Figure 4-4 Deformed shape of the wing in 3.0 rad/sec roll maneuver

The integrated air loads, in terms of shear force, bending and torsion moments, are shown in Figure 4-5 through Figure 4-7, respectively. The air load distributions due to the rolling velocity, p, are shown by thin solid lines, while the net load distributions are shown by heavy solid lines.

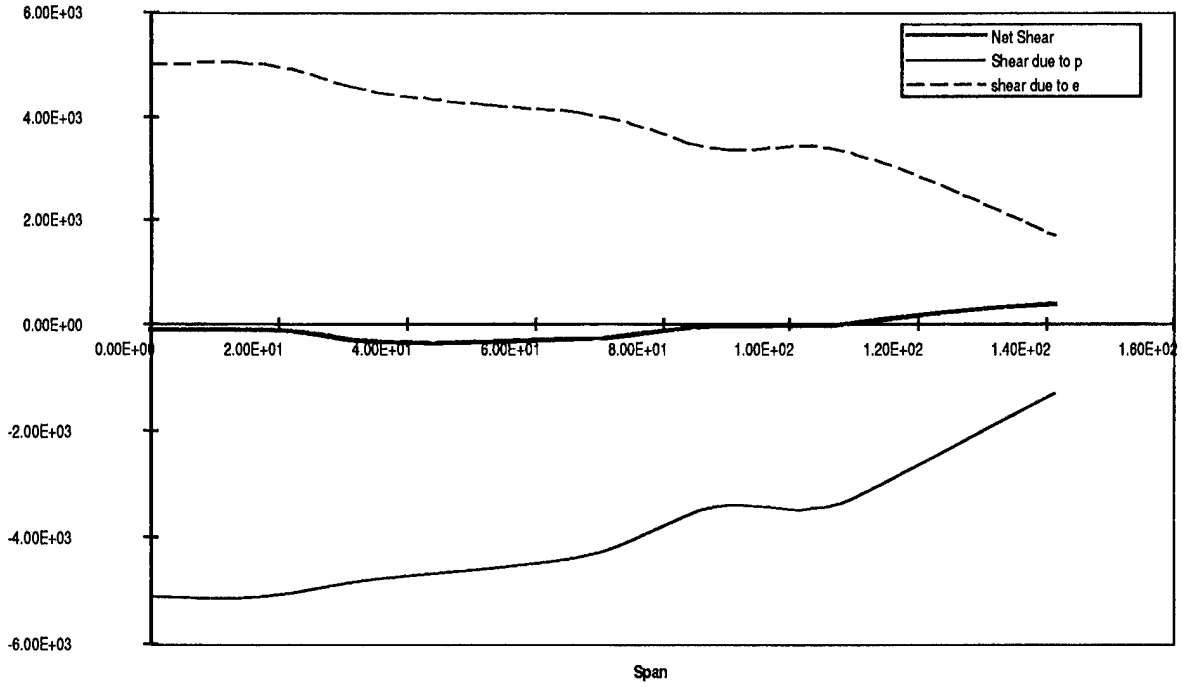

Figure 4-5 Shear load distribution along an elastic axis located at 40% chord. M=0.5 p=3.0 rad/sec roll maneuver at Sea level

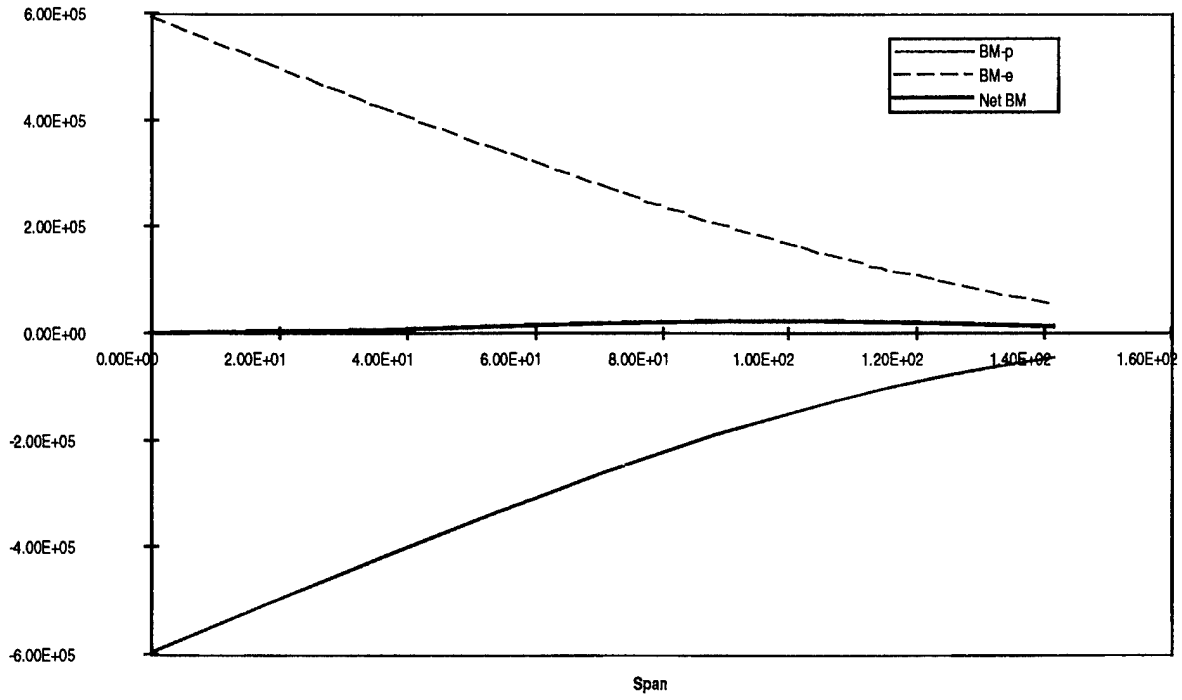

Figure 4-6 Bending moment and torsion distribution along an elastic axis located at 40% chord. M=0.5 p=3.0 rad/sec at Sea level

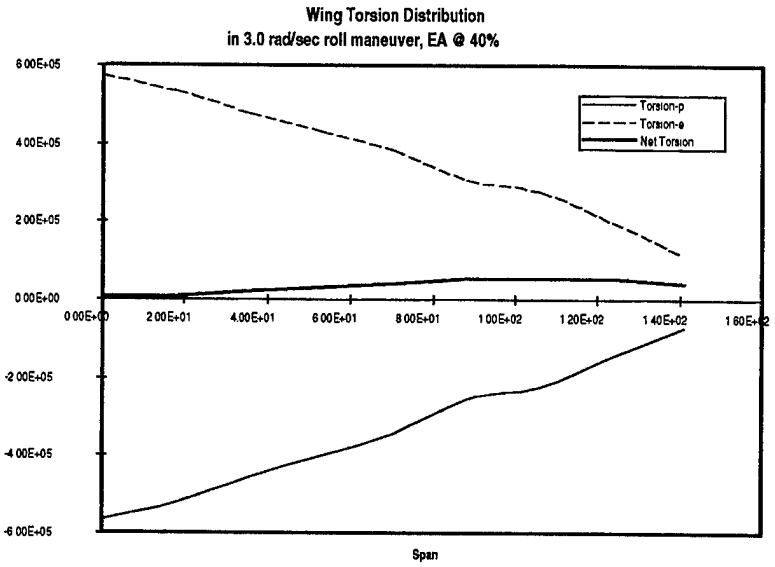

Figure 4-7 Torsion Moment distribution along an elastic axis located at 40% chord. M=0.5 p=3.0 rad/sec at Sea level

The inchworm type solid state actuators shown in Figure 4-2 are able to magnify the displacements by an order of magnitude. This is known as the mechanical advantage (MA). This is necessary to accommodate large relative displacements between the end points or the attachment points of the actuators. With this mechanism, relatively small-distributed forces will be able to deform the lifting surface so as to perform required flight maneuvers. Table 4-1 through 4-3 show the effect of the mechanical advantage on actuator power requirement and the net energy.

Figure 4-8 shows the energy required to perform a 3.0 radian/second roll versus the mechanical advantage of an actuator. For MA less than 100, a large amount of input power is required to stretch the actuator to match the relative displacement between the end points of the actuator. Otherwise, desired roll rate cannot be achieved. For actuators with MA greater than 400, the required energy is constant at 250 ft.lbs. This means the actuator is able to freely accommodate the expansion between the attachment points.

Mechanical Advantage = 100.0					
Net Energy = 1017.0 ft.lbs.					
Actuator Element	**Stimuli (Volt)**	**Stress (psi)**	**Force (lbs.)**	**Energy (in.lbs.)**	**Displacement (in.)**
1	22.20	-31,700.0	-1,590.0	40.0	0.600
2	-22.20	39,100.0	1,960.0	61.0	0.280
3	152.00	-284,000.0	-14,200.0	3,210.0	0.495
4	-112.00	217,000.0	10,900.0	1,880.0	0.026
5	110.00	-268,000.0	-13,400.0	2,870.0	-0.431
6	-104.00	249,000.0	12,500.0	2,470.0	-1.494
7	44.19	-133,566.6	-6,678.3	711.0	-1.520
8	-36.21	110,627.8	5,531.3	488.0	-2.930
9	29.65	-83,604.3	-4,180.2	279.1	-2.280
10	-24.56	72,489.1	3,624.5	209.8	-3.740

Table 4-1 The effect of mechanical advantage on the actuator energy requirement, MA = 100

Mechanical Advantage = 500.0					
Net Energy = 309.0 ft.lbs.					
Actuator Element	**Stimuli (Volt)**	**Stress (psi)**	**Force (lbs.)**	**Energy (in.lbs.)**	**Displacement (in.)**
1	5.200	-10,629.8	-531.50	4.50	0.598
2	-3.700	15,760.0	788.00	9.89	0.280
3	31.170	-132,418.1	-6,620.90	698.20	0.489
4	-21.570	103,784.2	5,189.20	428.90	1.941
5	22.800	-158,524.4	-7,926.20	1,002.20	-0.435
6	-19.900	143,892.8	7,194.64	825.70	-1.498
7	9.600	-90,266.0	-4,513.30	324.94	-1.514
8	-6.400	73,313.2	3,665.70	214.34	-2.921
9	6.700	-54,929.37	-2,746.50	120.50	-2.262
10	-4.096	46,892.9	2,344.64	87.79	-3.730

Table 4-2 The effect of mechanical advantage on the actuator energy requirement, MA = 500

Mechanical Advantage = 1000.0					
Net Energy = 251.0 ft.lbs.					
Actuator Element	**Stimuli (Volt)**	**Stress (psi)**	**Force (lbs.)**	**Energy (in.lbs.)**	**Displacement (in.)**
1	3.100	-8,150.1	-407.5	2.65	0.590
2	-1.330	12,911.8	645.6	6.64	0.270
3	16.030	113,551.6	5,677.6	513.40	0.480
4	-10.240	89,644.0	4,482.2	319.90	0.011
5	11.870	-144,634.7	-7,231.7	834.30	-0.440
6	-9.423	130,595.9	6,529.8	680.20	-1.500
7	5.290	-84,770.3	-4,238.5	286.60	-1.510
8	-2.700	68,567.6	3,428.4	187.50	-2.914
9	3.845	-51,337.5	-2,566.9	105.20	-2.240
10	-1.538	43,671.5	2,183.6	76.14	-3.710

Table 4-3 The effect of mechanical advantage On the actuator energy requirement, MA = 1000

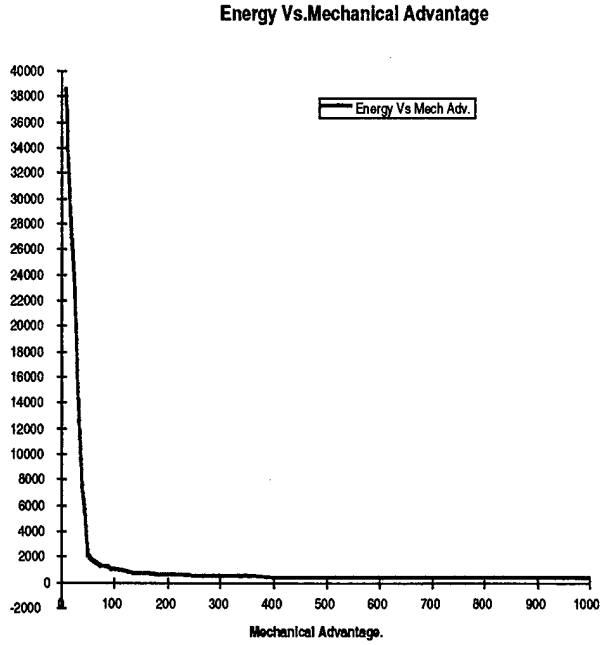

Figure 4-8 Actuator Energy vs. Mechanical Advantage.

4.3 Example 2: Symmetric Pull-up Maneuver

Two types of actuation systems were exercised. One involving the deformation of trailing edge control surface as depicted in Figure 4-2. Another actuation system was represented by a set of diagonal members placed along three rib sections near the wing tip as depicted in Figure 4-3. The relative merits of these two configurations are discussed next.

4.3.1 Case 1: Subsonic flow using the trailing edge control surface

Symmetric maneuver trim analysis of a typical fighter aircraft has been performed using 10 piezo-inchworm actuators as shown in Figure 4-2. The flight conditions were:

Gross weight of the aircraft	10978 lbs.
Load Factor	6.0 g
Mach Number	0.5
Altitude	Sea level
Flight Velocity	6698.7 in/sec
Target Pitch Rate	0.2884 rad/sec
Center of Gravity	40% mean chord
Allowable Actuator Strain	0.002 inch/inch

Table 4-4 Flight configuration data

A pull-up maneuver analysis was performed with the data shown Table 4-4. The results in terms of load distribution, actuator energy and deformed shape of the wing are presented next. The deformed shape of the lifting surface is shown in Figure 4-9. As expected the deformed surface is continuously smooth. The magnitude of the actuator forces and energy required to perform these flight maneuvers depends very much on the degree of satisfying the constraint by selecting the weighting coefficient Q. Large values of Q enforce the constraints very accurately, while smaller values satisfy within 10% of the desired values. Consider for example the constraint on the pitch rate

$$\varepsilon = \overline{q}_T - \overline{q} = 0$$

For large values of the weighting coefficient, Q, the constraint, ε, will be satisfied exactly. The actuator energy, force and stimuli for two values of Q are presented in Table 4-5.

Constraint Q	**Actuator Energy (Hp-hour)**	**Actuator Stimuli (Volts)**	**Actuator Force (lbs.)**	**Target pitch rate** $\overline{q}_T$	**Solution Pitch Rate** $\overline{q}$
Q = 1	E = 4.7e-08	V = 115	F = 66.37	0.00258	0.3531
Q = 10.0e+15	E = 2.797	V = 9.9e+06	F = 5.7e+06	0.00258	0.002584

Table 4-5 Effect of constraint weighting coefficients on power requirement

In the first case when the pitch rate is not enforced to match the required load factor the solution shows that only lift equilibrium is satisfied while the pitching moment remains unbalanced by a small amount. For this case the actuator input is 115 volt and the actuator develops 66.7 lbs. of force. This is an extremely small actuator input for an aircraft comparable to F16 to perform a 6.0g maneuver in symmetric flight.

On the other hand, to balance the pitching moment without a horizontal tail a large value of the weighting coefficient Q must be selected to enforce the solution pitch rate $\overline{q}$ to match its target value $\overline{q}_T$. This results in demanding extremely large actuator stimuli (electrical volts) and actuator forces as shown in the second row of Table . The actuators force the lifting surface to deform in an unusual configuration so that the resulting air load distribution satisfies both lift and pitch equilibrium.

The corresponding shear force, bending moment and torsion moment distributions are shown in Figure 4-10 through Figure **4-12**. The lift equilibrium, as seen in Figure 4-10, is achieved irrespective of what value of Q is used. While bending and torsion moments are different for these two cases.

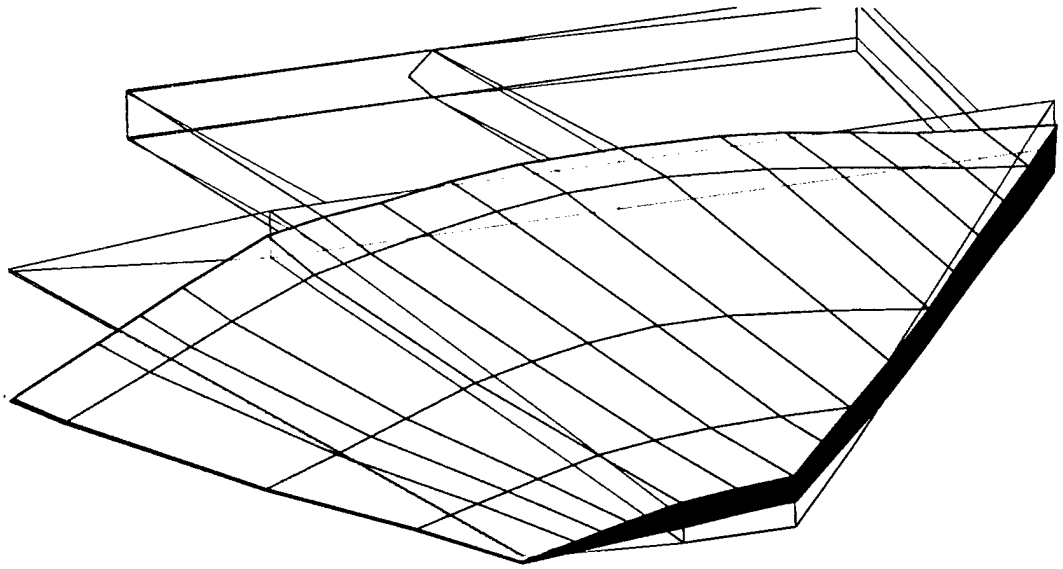

Figure 4-9 Deformed shape of the wing in 6.0g pull-up maneuver

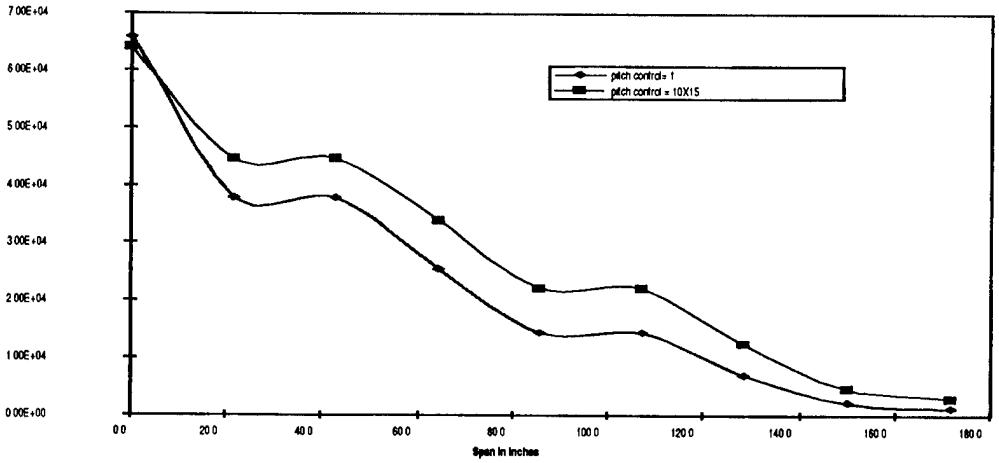

Figure 4-10 Shear Force Distribution in 6.0g pull-up maneuver

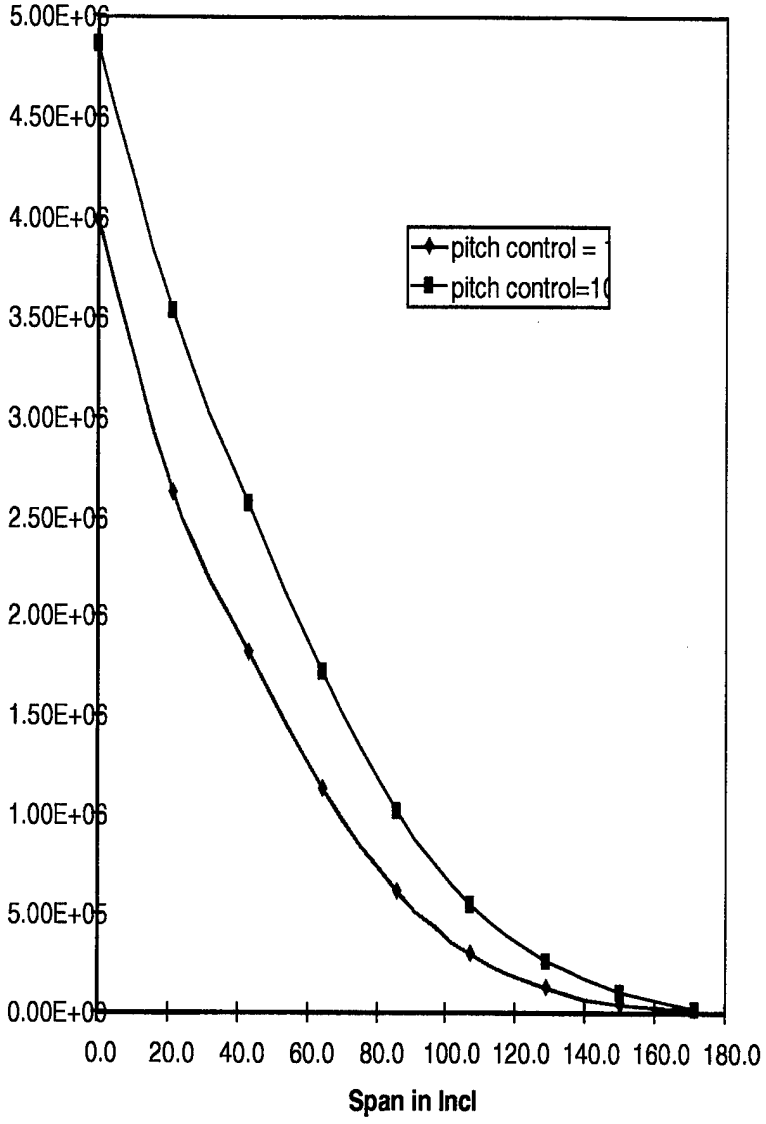

Figure 4-11 Bending moment distribution along wing span in 6.0g pull-up maneuver

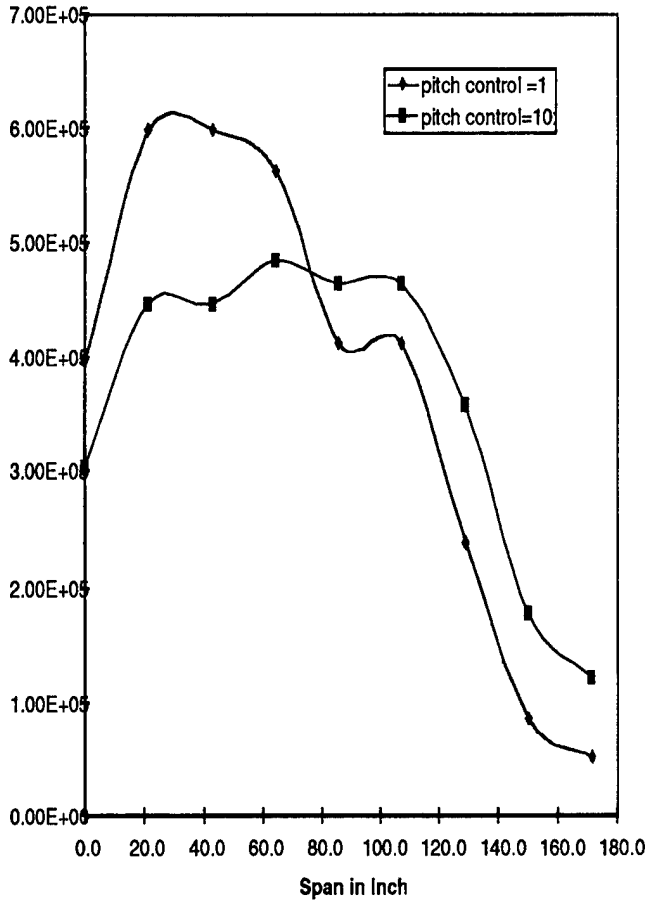

Figure 4-12 Torsion moment distribution along the wing span in 6.0g pull-up maneuver

4.3.2 Case 2: Supersonic flow using the trailing edge control surface

Another example, using the same aircraft configuration and flight conditions, was conducted in supersonic flow at Mach, M=1.2. The actuator energy requirement and actuator force data are presented in Table 4-6. In the supersonic case the unbalanced pitching moment is very small compared to that in the subsonic flow. Because, the aerodynamic center in supersonic flow lies downstream of the quarter chord and is closer to the center of mass of the aircraft. However, even though the unbalanced pitching moment is small, fairly large actuator stimuli and forces are required to satisfy the pitch rate exactly. The corresponding forces are presented in

Figure 4-13 through Figure **4-15**. Hardly any difference is seen in these plots for the two cases with Q=1 and Q=10e+15.

Constraint Q	Actuator Energy (Hp-hour)	Actuator Stimuli (Volts)	Actuator Force (lbs.)	Target pitch rate $\overline{q}_T$	Solution Pitch Rate $\overline{q}$
Q = 1	E = 5.3e-08	V = 114.0	F = 65.29	0.000448	0.005501
Q = 10.0e+15	E = 4.44e-04	V = 9.3e+04	F = 6.9e+04	0.000448	0.0004481

Table 4-6 Effect of constraint weighting coefficients on power requirement

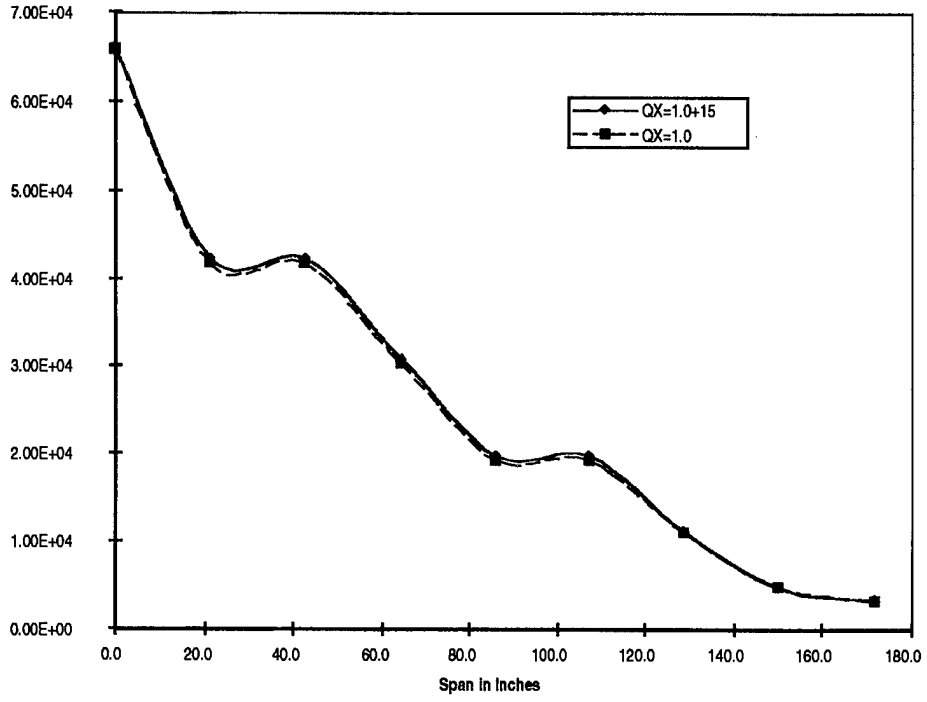

Figure 4-13 Shear force distribution along the wing span in 6.0g pull-up maneuver, M=1.2

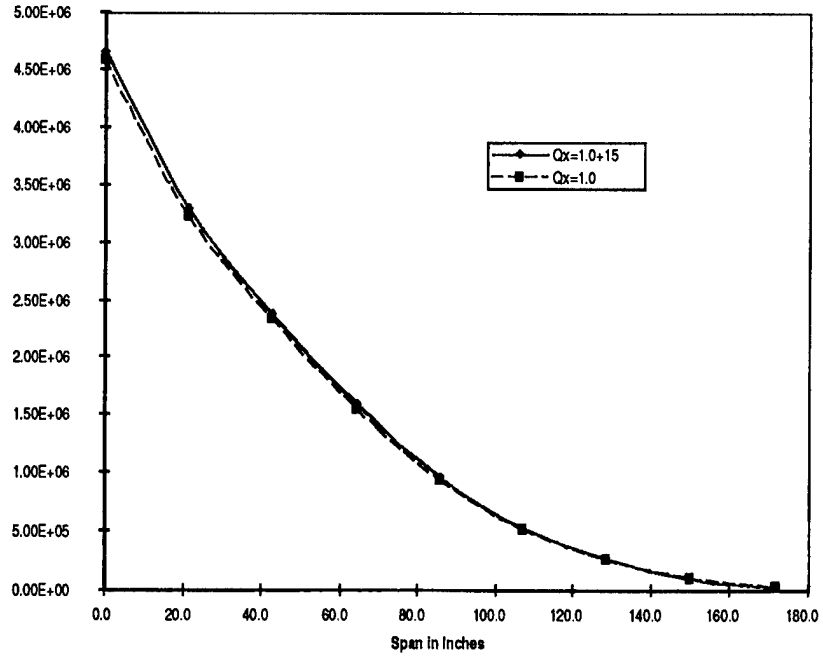

Figure 4-14 Bending moment distribution along wing span in 6.0g pull-up maneuver, M=1.2

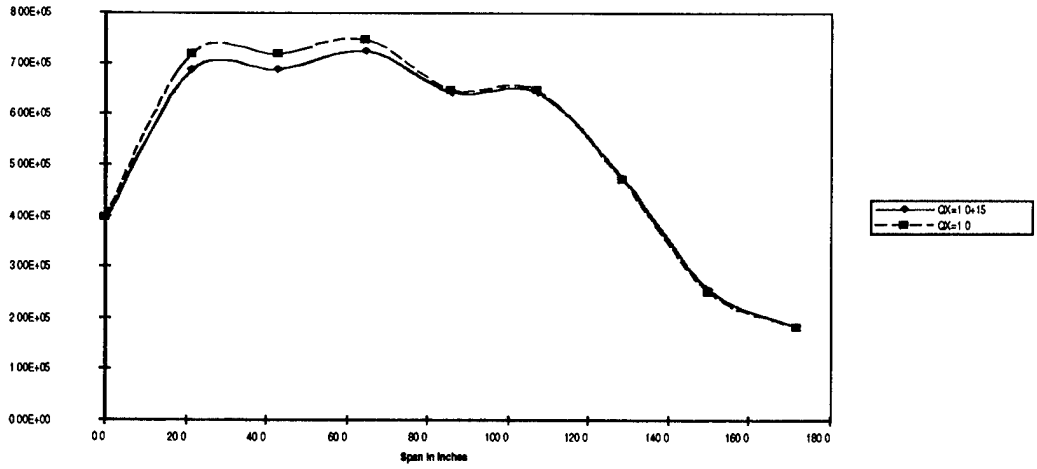

Figure 4-15 Torsion moment distribution along wing span in 6.0g pull-up maneuver, M=1.2

4.3.3 Case 3: Supersonic flow using distributed diagonal actuators

In order to understand the nature and merits of distributed actuators compared to the conventional aerodynamic effectors, a set of actuators was placed diagonally at three rib stations near the wing tip.

The aircraft configuration was the same as in case 2 except that the diagonal actuators were used instead of the trailing edge effectors. The actuator stimuli, forces and energy for two constraint conditions with Q = 1 and Q = 10.0e+15 are presented in Table 4-7. The corresponding load distributions in terms of shear, bending moment and torsion are shown in Figure 4-16 through Figure 4-18, respectively. The deformed shape of the wing is depicted in Figure 4-19 and Figure 4-20. It is intriguing to compare the power and load distributions in two cases, trailing edge effector case and the diagonal actuation system. When Q=1 the power required in both cases was practically the same. However, the trailing edge effector case had smaller unbalanced pitching moment. In other words it gave the air load distribution which was closer to the trimmed condition both in lift and pitch. Hence, the air load distributions in Figures 4-13 through 4-15 show very little difference between two values of Q.

Constraint Q	**Actuator Energy (Hp-hour)**	**Actuator Stimuli (Volts)**	**Actuator Force (lbs.)**	**Target pitch rate** $\overline{q}_T$	**Solution Pitch Rate** $\overline{q}$
Q = 1	4.55e-09	63.39	62.5	0.000448	0.04257
Q=10.0e+15	4.1449e-02	14.67e+04	14.47e+04	0.000448	0.0004481

Table 4-7 Effect of constraint weighting coefficients on power requirement

On the other hand the diagonally distributed actuator system shows drastically different air load distributions as depicted in Figure 4-16, Figure 4-17, and Figure 4-18. The lift distribution moves towards the wing root resulting in reduced wing root bending moment by about 50%.

The deformed shape of the wing corresponding to 6.0 g pull-up maneuver in supersonic speed, M=1.2 is depicted in Figure 4-19 and Figure 4-20. Figure 4-19 shows the view looking from the trailing edge, while Figure 4-20 shows the view from the wing tip.

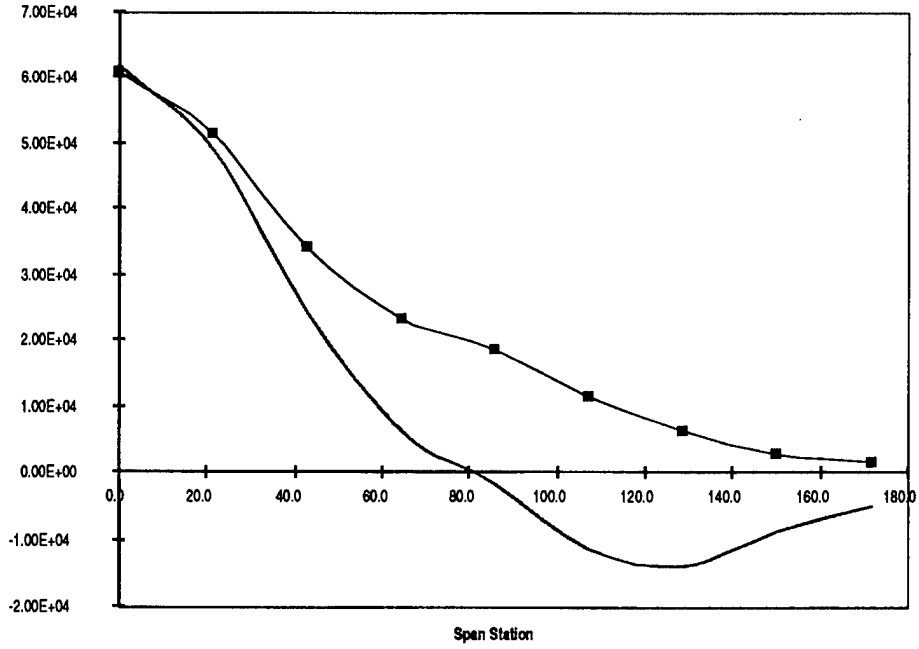

Figure 4-16 Shear force distribution along wing span
in 6.0g pull-up maneuver, M=1.2

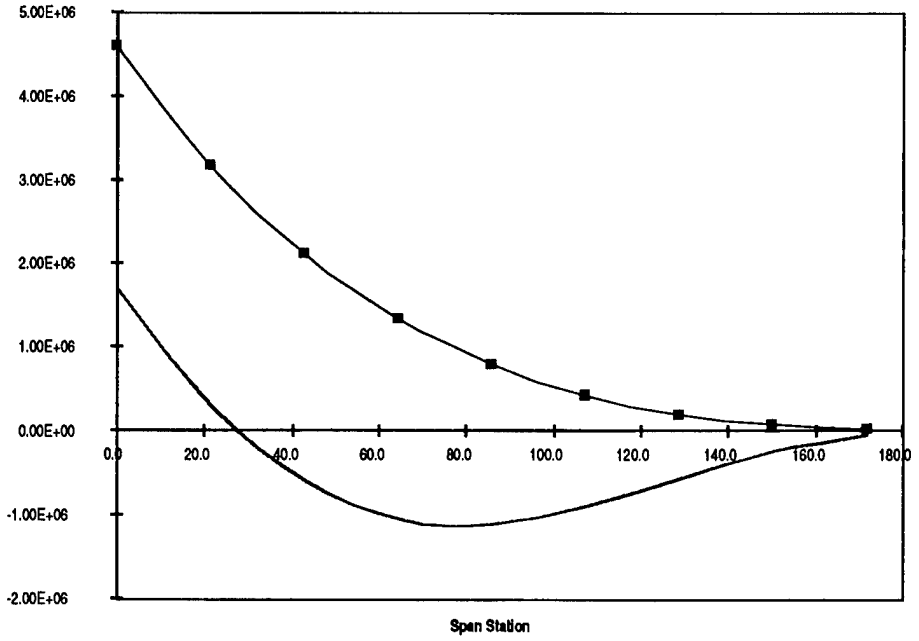

Figure 4-17 Bending moment distribution along the wing span
6.0g pull-up maneuver, M=1.2

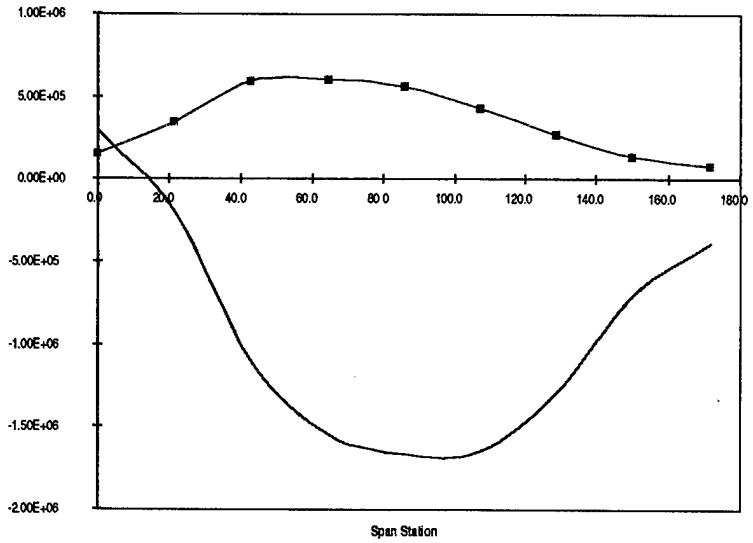

Figure 4-18 Torsion distribution along the wing span
6.0g pull-up maneuver, M=1.2

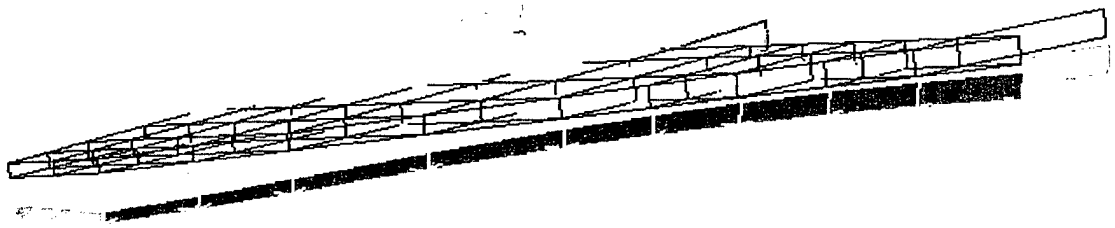

Figure 4-19 Deformed shape of the wing due to diagonal actuation system looking from the trailing edge

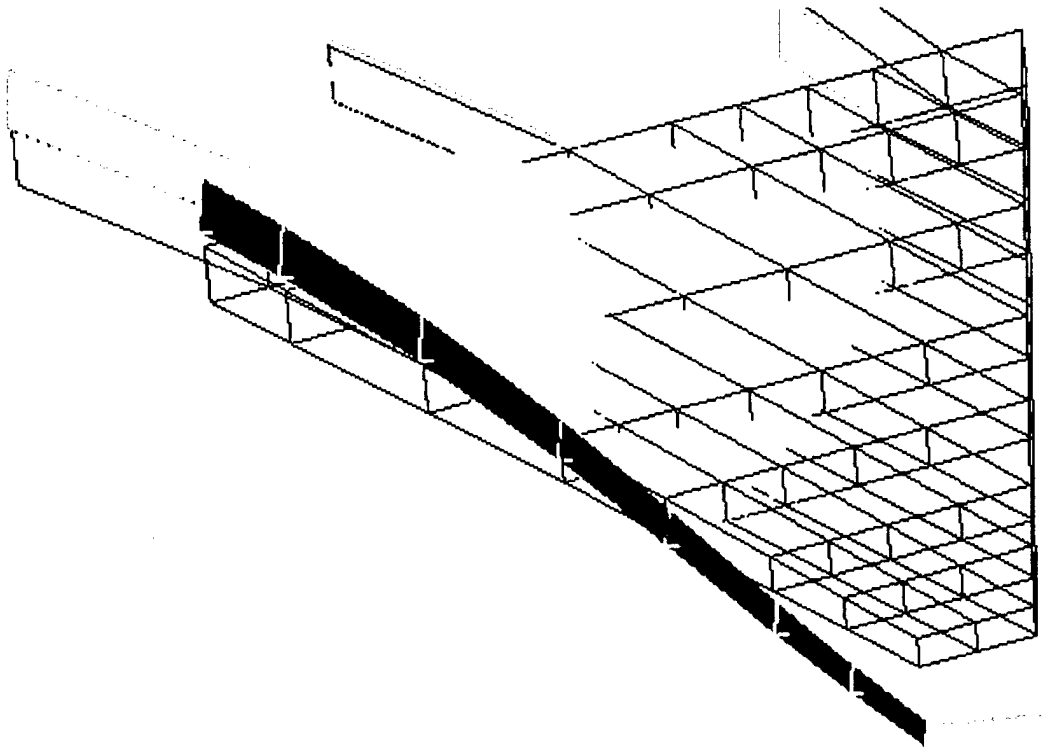

Figure 4-20 Deformed shape of the wing due to diagonal actuation system looking from the wing tip

5. Conclusions and Recommendations

An analytical simulation algorithm based on the optimal control theory has been developed to compute flight maneuver loads using solid state actuators. A state space formulation including unsteady air loads and closed loop control laws has been derived. Aeroelastic analyses and aircraft flight dynamics can be performed. A few flight maneuvers have been conducted in 1.0g roll and 6.0g pull-up both in subsonic and supersonic flow conditions. This study suggests that the solid state actuators must be able to travel large distances between contact points for minimum actuator power. Large displacements and forces are achievable in piezoelectric devices such as the inchworm actuators. To perform pull-up and pushover maneuvers a canard or horizontal tail type secondary load carrying devices are required so that actuator power requirement will be a minimum.

6. REFERENCES

1. Wong, K. J., "AFTI/F-111 Mission Adaptive Wing Lift and Drag Flight Test Results," AFFTC-TR-87-02, Final Report, April 1987.

2. Hall, J, M., "Executive Summary AFTI/F-111 Mission Adaptive Wing," WRDC-TR-89-3083, September 1989.

3. Cogburn, L. T., "AFTI/F-111 Mission Adaptive Wing Flutter and Aeroservoelastic Test Program," AFFTC-TR-86-42, Final Report, March 1987.

4. Appa, K., Martin, C. A., Scherer, L. B., and Kudva, J. N.. "Aerodynamic Benefits of Hingeless Control Surfaces," SPIE Far East and Pacific Rim Symposium on Smart Materials and Structures, December, 11-14, 1996, Indian Institute of Science Bangalore, India.

5. Appa, K. "Recent Advances in Manoeuvre Loads Analysis," Computer Methods in Applied Mechanics and Engineering, Volume 90, Nos. 1-3, 1991, pp. 693-717.

6. Appa, K., and Argyris, J. "Computational Aircraft Dynamics and Loads," Sadhana, Vol. 19, Part 3, June 1994, pp. 467-485, Academy Proceedings in Engineering Sciences, Printed in India.

7. Appa, K., Argyris, J., Guruswamy, G. P., and Martin, C. A., "Synergistic Aircraft Design Using CFD Air Loads," AIAA-96-4057-CP, 6th AIAA/NASA/USAF Multidisciplinary Analysis & Optimization Symposium, September 4-6,1996, Bellevue, WA.

8. Khot, N. S., Eastep, F. E., and Kolonay, R. M., "Optimization of a Composite Wing Structure for Enhancement of the Rolling Maneuver," AIAA-96-3998-CP, 6th AIAA/NASA/USAF Multidisciplinary Analysis & Optimization Symposium, September 4-6,1996, Bellevue, WA.

9. Appa, K., "Maneuver Loads Analysis for Military Aircraft", Section 6, Chapter 5, in Flight-Vehicle Materials, Structures, and Dynamics - Assessment and Future Directions, Vol. 1, Editors: A.K. Noor and S.L. Venneri, Published by the American Institute of Mechanical Engineers, New York, NY, 10017, 1994.

10. Appa, K., Ausman, J., and Khot, N. S., Feasibility Assessment and Optimization of Smart Actuation Systems for Enhanced Aircraft Maneuver Performance, Flight Dynamics Directorate, WL-TR-97-3083, July 1997.